

Exploring the Spectral Shape of Gravitational Waves Induced by Primordial Scalar Perturbations and Connection with the Primordial Black Hole Scenarios

Ioannis Dalianis^{1,*} and Konstantinos Kritos^{1,†}

¹*Physics Division, National Technical University of Athens, 15780 Zografou campus, Athens, Greece*

There is a growing expectation that the gravitational wave detectors will start probing the stochastic gravitational wave backgrounds in the following years. We explore the spectral shapes of gravitational waves induced to second order by scalar perturbations and presumably have been produced in the early universe. We calculate the gravitational wave spectra generated during radiation and kination eras together with the associated primordial black hole counterpart. We employ power spectra for the primordial curvature perturbation generated by α -attractors and nonminimal derivative coupling inflation models as well as Gaussian and delta-type shapes. We demonstrate the ability of the tensor modes to constrain the spectrum of the primordial curvature perturbations and discriminate among inflationary models. Gravitational wave production during kination and radiation eras can also be distinguished by their spectral shapes and amplitudes.

I. INTRODUCTION

A network of operating and designed gravitational wave detectors raise expectations that, sooner or later, the relic gravitational radiation background will be detected. Gravitational waves (GWs) are thought to be generated by several processes in the early universe [1–3]. Among them there is a model independent source, the primordial density scalar perturbations, that unambiguously source tensor modes at second order perturbation theory [4–8], the so-called induced gravitational waves (IGW).

Tensor modes are induced to second order by scalar perturbations despite their decoupling at first order. The cosmological implications of the scalar induced GWs to second order were first discussed in the pioneering works [9], where the effects of IGWs on cosmic microwave background (CMB) polarization was computed, and [10], where the spectrum of the IGWs on small scales was studied. Further notable results followed that extended our understanding and formulation of IGW physics [11–13] and gave us insights of how to probe the primordial power spectrum, $\mathcal{P}_{\mathcal{R}}(k)$, at small scales.

Primordial scalar density perturbations are directly measured only at the very large scales of the CMB with wave number $k_{\text{cmb}} \sim 10^{-2} \text{ Mpc}^{-1}$ and with amplitude $\delta\rho/\rho \sim 10^{-5}$. At smaller scales $k \gg k_{\text{cmb}}$ there are weak constraints coming mainly from bounds on the abundance of primordial black holes (PBHs) [14–16]. Additional constraints on the scalar density amplitude can come from gravitational wave experiments. Already, at the frequency range $f \sim 10^{-9} \text{ Hz}$ and $f \sim 10^2 \text{ Hz}$ the PTA and LIGO/VIRGO experiments, respectively, have provided upper bounds.

The weak bounds on the primordial $\mathcal{P}_{\mathcal{R}}(k)$ has prompted the building of several scenarios that exhibit an enhanced power at small scales. A subclass of these

scenarios predicts a significant PBH abundance, see Ref. [17] for a review. The new observational window to the very early universe through the IGWs can test these scenarios [18–37]. The interpretation of a GW signal is nevertheless a nontrivial task and one needs to take into account several parameters, such as the reheating temperature and the equation of state of the early universe, as well as whether the primordial fluctuations are Gaussian or a non-negligible non-Gaussianity exists [22, 25, 28, 38]. From a different point of view, detection of the relic GWs stochastic background is a direct probe of the very early cosmic history, which is unknown for $t \lesssim 1 \text{ s}$ [39]. In this context, the recent works [40–43] have studied the impact of different early cosmological evolution on the IGWs.

In this work we explore the shape of the IGWs produced in the early universe assuming different scenarios and models. Prior to BBN there are no direct tests of the thermodynamical state of the universe and we choose to presume either the standard radiation equation of state or that of the stiff fluid, as benchmark cases. We make a step forward compared to previous works taking into account the transition details from kination to radiation. We focus on a $\mathcal{P}_{\mathcal{R}}(k)$ shape with a peak. $\mathcal{P}_{\mathcal{R}}(k)$ with a peak is a rather interesting scenario because it predicts IGWs and might also generate PBHs that can be part of the dark matter in the galaxies. We target at cosmological parameter values that can be tested by the existing and designed GW experiments, such as LIGO and Laser Interferometer Space Antenna (LISA). We utilize Dirac δ and Gaussian-type $\mathcal{P}_{\mathcal{R}}(k)$ shapes and give a simple analytic expression for the energy density parameter of the IGWs, $\Omega_{\text{IGW}}(t_0)$, produced during radiation and kination regime.

Furthermore, we derive the scalar-induced GW spectral shapes for particular models of inflation: two α -attractors inflation models [44] and a generalized Galileon-type [45–47] model of inflation. We focus on particular three models [48–50] because each model yields a $\mathcal{P}_{\mathcal{R}}(k)$ with a different shape form: different width and scaling both in the IR and UV part of the scalar spectrum. We compare features of the $\mathcal{P}_{\mathcal{R}}(k)$ spectral

* dalianis@mail.ntua.gr

† ge16004@central.ntua.gr

shape with the corresponding $\Omega_{\text{IGW}}(f)$, examining the amplitudes and the scaling. This approach makes possible a demonstrative exploration of the IGW spectra with different shapes. A similar study in this direction has been performed in Refs. [51, 52] where, following analytic steps, general features of the IGW spectrum have been also described. Our analysis provides observational tests for this sort of viable inflation models as well.

In addition to the IGW spectra we examine the abundance and distribution of the PBHs associated with the $\mathcal{P}_{\mathcal{R}}(k)$. We examine scenarios that predict a sizable amount of both PBHs and IGWs, and scenarios that predict significant IGWs with the PBH counterpart being either negligibly small or promptly evaporating. We present analytic and numerical results and we manifest the connection between the PBH mass and the GW counterpart making use of figures and tables.

The paper is organized as follows. In Sec. II, we review the method that is usually followed in the literature to calculate the spectra of scalar-induced GWs. In Sec. III we focus on particular inflationary models that predict $\mathcal{P}_{\mathcal{R}}(k)$ with a peak as well as general Gaussian $\mathcal{P}_{\mathcal{R}}(k)$ types, and we specialize into radiation and kination domination early universe scenarios. In Sec. IV we turn into the PBH counterpart and calculate mass distributions and abundances. Our results are presented in Sec. V, and finally, in Sec. VI we draw our conclusions.

II. METHODOLOGY FOR CALCULATING INDUCED GRAVITATIONAL WAVES

In this section we review the formulas required to calculate the energy density of the induced gravitational waves (IGWs) by first order scalar perturbations and adjust the notation in our context. We follow Ref. [53] and for a further study in a relevant context we refer the reader to [42, 52, 53].

We consider a flat Friedmann-Robertson-Walker model with first order scalar perturbations Φ , Ψ and second order (induced) tensor perturbations h_{ij} , and ignore vector perturbations and first order tensor perturbations. We describe our perturbations in the Newtonian gauge. The

line element of the perturbed metric is written as,

$$ds^2 = a^2(\eta) \left[- (1 + 2\Phi) d\eta^2 + ((1 - 2\Psi) \delta_{ij} + \frac{1}{2} h_{ij}) dx^i dx^j \right], \quad (1)$$

where $a(\eta)$ is the scale factor and δ_{ij} is the Kronecker tensor. For future reference we also denote the conformal Hubble function by $\mathcal{H}(\eta) \equiv \frac{a'(\eta)}{a(\eta)}$. Here, and later, prime (') denotes conformal time differentiation. We will also ignore anisotropies¹ and set $\Phi = \Psi$. In the Newtonian gauge the scalar perturbations play the role of the gravitational potential and the tensor modes describe gravitational waves.

We define $x \equiv k\eta$ and express the evolution of the scalar perturbations in terms of the scalar transfer function, Φ , defined by $\Phi_{\mathbf{k}}(\eta) \equiv \Phi(x) \phi_{\mathbf{k}}$ in momentum space, where $\phi_{\mathbf{k}}$ the Fourier mode of the primordial scalar perturbations. Considering the field equations of general relativity for a single perfect cosmological fluid with the standard density-pressure equation of state (EOS) relation $p = w\rho$, the evolution equations for the gravitational potential is obtained by

$$\Phi''(x) + 3(1 + w) \mathcal{H}(\eta) \Phi'(x) + w k^2 \Phi(x) = 0. \quad (2)$$

We consider adiabatic perturbations (zero entropy perturbations) and initial conditions $\Phi(0) = 1$ and $\Phi'(0) = 0$ for the scalar transfer function. The general solution² of Eq. (2) is given in terms of the Bessel function of the first kind, J , and the gamma function, Γ , [12],

$$\Phi(x) = \frac{2^\alpha \Gamma(\alpha + 1)}{(\sqrt{w}x)^\alpha} J_\alpha(\sqrt{w}x), \quad (3)$$

where $\alpha = \frac{5+3w}{2(1+3w)}$.

The evolution of the induced tensor modes is given by the equation,

$$h_{\mathbf{k}}''(\eta) + 2\mathcal{H}(\eta)h_{\mathbf{k}}'(\eta) + k^2 h_{\mathbf{k}}(\eta) = \mathcal{S}_{\mathbf{k}}(\eta), \quad (4)$$

where the source function $\mathcal{S}_{\mathbf{k}}$ at the left-hand side plays a critical role. It is a convolution of scalar perturbations at different wave numbers given by

$$\mathcal{S}_{\mathbf{k}}(\eta) = 4 \int \frac{d^3q}{(2\pi)^{3/2}} e^{ij}(\mathbf{k}) q_i q_j \phi_{\mathbf{k}} \phi_{\mathbf{k}-\mathbf{q}} \times f(|\mathbf{q}|/k, |\mathbf{k}-\mathbf{q}|/k, \eta, k). \quad (5)$$

Here, e^{ij} is the polarization tensor, and f is an auxiliary function defined by

¹ For the effects of the anisotropic stress due to $\mathcal{O}(10)\%$ difference between Φ and Ψ see Ref. [12].

² Here, we neglect the contribution from the Bessel function of the

second kind, $Y_\alpha(\sqrt{w}x)$, to avoid the singularity at $\eta = 0$.

$$f(u, v, \eta, k) = 2 \Phi(ux) \Phi(vx) + \frac{4}{3(1+w)} \left[\Phi(ux) + \frac{uk}{\mathcal{H}(\eta)} \Phi'(ux) \right] \left[\Phi(vx) + \frac{vk}{\mathcal{H}(\eta)} \Phi'(vx) \right]. \quad (6)$$

Gaussian fluctuations are best described with the power spectral density. For scalar and tensor perturbations the power spectral densities, called \mathcal{P}_Φ and \mathcal{P}_h , respectively, are defined in terms of two point correlation functions as

$$\langle \phi_{\mathbf{q}} \phi_{\mathbf{k}} \rangle \equiv \frac{2\pi}{k^3} \mathcal{P}_\Phi(k) \delta^{(3)}(\mathbf{q} + \mathbf{k}), \quad (7)$$

and

$$\langle h_{\mathbf{q}}^{\oplus, \otimes}(\eta) h_{\mathbf{k}}^{\oplus, \otimes}(\eta) \rangle \equiv \frac{2\pi}{k^3} \mathcal{P}_h(\eta, k) \delta^{(3)}(\mathbf{q} + \mathbf{k}), \quad (8)$$

where $\delta^{(3)}$ is the three-dimensional delta distribution and \oplus, \otimes denote the two polarization modes. The power spectral density of the comoving curvature perturbation, $\mathcal{P}_\mathcal{R}$, is related to \mathcal{P}_Φ via

$$\mathcal{P}_\mathcal{R}(k) = \left(\frac{5+3w}{3+3w} \right)^2 \mathcal{P}_\Phi(k). \quad (9)$$

The density parameter of IGWs is defined to be the ratio of the energy density in IGWs over the total energy density, taking into account both \oplus and \otimes GW polarizations. A useful definition for the energy density of IGWs per unit logarithmic frequency interval is given in terms of the tensor power spectrum as

$$\Omega_{\text{IGW}}(\eta, k) \equiv \frac{1}{24} \left(\frac{k}{\mathcal{H}(\eta)} \right)^2 \overline{\mathcal{P}_h(\eta, k)}, \quad (10)$$

where the overline denotes the oscillation average. The power spectral density of the tensor perturbations is expressed as a double integral involving the power spectrum of the curvature perturbations,

$$\overline{\mathcal{P}_h(\eta, k)} = \int_0^\infty dv \int_{|1-v|}^{1+v} du \mathcal{T}(u, v, \eta, k) \mathcal{P}_\mathcal{R}(uk) \mathcal{P}_\mathcal{R}(vk). \quad (11)$$

The \mathcal{T} is the tensor transfer function given by

$$\mathcal{T}(u, v, \eta, k) = 4 \left(\frac{4v^2 - (1 + v^2 - u^2)^2}{4uv} \right)^2 \times \left(\frac{3+3w}{5+3w} \right)^2 \overline{I^2(u, v, \eta, k)}, \quad (12)$$

where we have defined the kernel function by

$$I(u, v, \eta, k) = \int_0^x dy \frac{a(y/k)}{a(\eta)} k G_k(x, y) f(u, v, y/k, k), \quad (13)$$

and have used the Green's function $k G_k$ given in terms of Bessel functions, as $k G_k(x, y) = \frac{\pi}{2} \sqrt{x y} \cdot$

$[Y_\nu(x) J_\nu(y) - Y_\nu(y) J_\nu(x)]$, with $\nu \equiv \frac{3(1-w)}{2(1+3w)}$, [54]. The oscillation average is given by

$$\overline{I^2(u, v, \eta, k)} \equiv \frac{1}{2\pi} \int_x^{x+2\pi} dy I^2(u, v, \eta, y/\eta). \quad (14)$$

The IGWs are sourced gravitational waves. At the time t_c the production of IGWs ceases and afterward the GWs propagate freely. In a radiation dominated background the energy density parameter of the GWs also remains constant. The energy density parameter of the IGW today, t_0 , is therefore given by Eq. (10) at the moment t_c times the current radiation density parameter, $\Omega_{\gamma,0} h^2 = 4.2 \times 10^{-5}$, modulo changes in the number of the relativistic degrees of freedom g_* in the radiation fluid,

$$\Omega_{\text{IGW}}(t_0, f) h^2 = 0.39 \times \left(\frac{g_*}{106.75} \right)^{-\frac{1}{3}} \Omega_{\gamma,0} h^2 \times \Omega_{\text{IGW}}(t_c, f). \quad (15)$$

For the total IGW density parameter, we integrate Eq. (15) over the logarithmic interval of frequency,

$$\Omega_{\text{IGW}}(t_0) = \int_{f_{\min}}^{f_{\max}} d \ln f \Omega_{\text{IGW}}(t_0, f). \quad (16)$$

Since our spectra will be peaked at some frequency $f_{\text{IGW}}^{\text{P}}$ we may take $f_{\min} = f_{\text{IGW}}^{\text{P}}/100$ and $f_{\max} = 10 f_{\text{IGW}}^{\text{P}}$. Here $\Omega_{\text{IGW}}(t_0)$ should not be confused with $\Omega_{\text{IGW}}(t_0, f)$ where the later function is frequency dependent and denotes the density parameter of IGWs per logarithmic frequency interval.

In the following we will examine particular $\mathcal{P}_\mathcal{R}(k)$ types and we will focus on two benchmark early universe cosmological scenarios: the radiation and kination dominated eras.

III. STUDY OF THE IGWs PRODUCED BY EXPLICIT MODELS AND IN DIFFERENT COSMOLOGICAL ERAS

It is well known that the equation of state of the Universe has not been directly probed for times prior to BBN $t \sim 1$ s. IGWs have amplitude and spectral shape that depend on the details of cosmological era at the time of their production. Indeed, the Φ that sources the GWs evolves in a different way for different equation of state w and, additionally, the energy density of the produced GWs scales differently with respect to the background.

In order to study the IGW spectrum and demonstrate its properties and behaviour we assume that the curvature power spectrum $\mathcal{P}_\mathcal{R}(k)$ features a peak at the wave

number k_p . If the amplitude of the $\mathcal{P}_{\mathcal{R}}(k)$ peak is significant it produces a strong IGW signal, that is possibly detectable, and additionally, enhances exponentially the production probability for PBHs. Therefore, explicit models can be tested and upper bounds on the IGWs can be derived.

We will study $\mathcal{P}_{\mathcal{R}}(k)$ peaks generated by complete and explicit inflationary models, namely the α -attractors and Horndeski general nonminimal derivative coupling (GNMDC) inflation introduced in Refs. [48] and [50] respectively. The qualitative element of the first model is that features a near-inflection point [55–58] and the second model features a so-called high friction regime [59]. From the structural side the two inflationary models [48, 50] have a noncanonical kinetic term,

$$\frac{\mathcal{L}^{\alpha\text{-attractors}}}{\sqrt{-g}} = \frac{R}{2} - \frac{(\partial_\mu \tilde{\varphi})^2}{2(1 - \frac{\tilde{\varphi}^2}{6\alpha})^2} + V(\tilde{\varphi}) \quad (17)$$

$$\frac{\mathcal{L}^{\text{GNMDC}}}{\sqrt{-g}} = \frac{R}{2} - \hat{f}(\varphi) G^{\mu\nu} \partial_\mu \varphi \partial_\nu \varphi + V(\varphi) \quad (18)$$

We note that we examine the second order induced tensor perturbations, not the first order tensor modes produced by the inflationary stage itself; for the latter, see e.g., [60, 61] for relevant studies. What is of interest for our analysis is that, respectively, the form of the α -attractor potential and the form of the GNMDC coupling can generate an enhanced $\mathcal{P}_{\mathcal{R}}(k)$ spectrum at k_p and with a variety of shape forms. The α -attractors potentials that we utilize generate $\mathcal{P}_{\mathcal{R}}(k)$ slopes that increase like k^3 and k^4 and decrease like k^{-1} or k^{-4} . On the other hand the $\mathcal{P}_{\mathcal{R}}(k)$ slopes of the Galileon GNMDC model increase like k^2 and k^4 and decrease like k^{-4} . For a comprehensive description and details about the inflationary Lagrangians (17) and (18), as well as the generated $\mathcal{P}_{\mathcal{R}}(k)$ shapes we refer the reader to the original works [48, 50]. A brief description can be found in Appendix B.

Moreover, irrespective of the inflationary theory, we assume general shapes for the $\mathcal{P}_{\mathcal{R}}(k)$ spectra. We utilize Gaussian and Dirac δ -type distributions,

$$\mathcal{P}_{\mathcal{R}}^G(z) = A_{\mathcal{R}} e^{-(z/\epsilon)^2} = \frac{A_0}{\epsilon\sqrt{\pi}} e^{-(z/\epsilon)^2} \quad (19)$$

$$\mathcal{P}_{\mathcal{R}}^D(z) = A_0 \delta(z) \quad (20)$$

where $z \equiv \ln(k/k_p)$ and $A_{\mathcal{R}} = \mathcal{P}_{\mathcal{R}}(k_p)$. In the limit $\epsilon \rightarrow 0$ the Gaussian distribution approaches the δ -distribution. The advantage of these distributions is that analytic or semianalytic results can be obtained and, in addition, realistic models can be parametrized. Gaussian spectra have been also studied recently in [52].

We are interested in three characteristics for the power spectra $\mathcal{P}_{\mathcal{R}}(k)$: i) the amplitude $A_{\mathcal{R}}$; ii) the wave number of the peak, k_p , where $\mathcal{P}_{\mathcal{R}}(k_p) = A_{\mathcal{R}}$; and iii) the width ϵ . We choose a large amplitude $A_{\mathcal{R}}$ so that the IGW signal is significant. We slightly modulate the $A_{\mathcal{R}}$ in order to maximize or minimize to a negligible amount the PBH abundance. The wave number k_p is chosen so that either the PBHs constitute a significant fraction of the dark matter in the galaxies, or the frequency of the IGWs lays in the sensitivity range of the gravitational detectors.

Let us now examine two benchmark cosmological scenarios separately: the radiation and the kination.

A. The radiation domination scenario

Let us assume that the $\mathcal{P}_{\mathcal{R}}(k)$ peak enters the horizon during the radiation era. This is the standard early universe cosmological scenario. The IGWs produced during radiation era have been thoroughly studied, thus, we will not repeat known results and technical details. We remind the reader that the potential $\Phi(x)$ oscillates with a x^{-2} decaying amplitude in subhorizon scales. The formalism of the Sec. II is applied for $w = 1/3$. We quote the analytic expression that we use to obtain the IGWs results for the models (17), (18) and (19). Relying on analytical methods, we obtain the tensor transfer function in late times as was done in [53]; the resulting expression is

$$\lim_{x \rightarrow \infty} x \mathcal{T}_{\text{RD}}(u, v, x) = 2 \left(\frac{4v^2 - (1 + v^2 - u^2)^2}{4uv} \right)^2 \left(\frac{3(u^2 + v^2 - 3)}{4u^3v^3} \right)^2 \left[\left(-4uv + (u^2 + v^2 - 3) \ln \left| \frac{3 - (u+v)^2}{3 - (u-v)^2} \right| \right)^2 + \pi^2 (u^2 + v^2 - 3)^2 \Theta(u + v\sqrt{3}) \right] \quad (21)$$

where Θ is the unit step function.

We then perform a numerical integration to calculate the $\mathcal{P}_h(\eta, k)$ as Eq. (11) dictates. In order for this to be

done, an input for the power spectrum shape $\mathcal{P}_{\mathcal{R}}(k)$ is required. We assume two Gaussian power spectra with medium and narrow widths, $\epsilon = 1$ and $\epsilon = 0.1$, respec-

tively, as well as power spectra produced by α -attractor and Horndeski-type inflationary theories; see Fig. 4. The $\mathcal{P}_{\mathcal{R}}(k)$ produced by these inflationary theories is found after solving the Mukhanov-Sasaki equation numerically.

B. The kination domination scenario

In this subsection, let us assume the cosmological scenario that the very early universe has been dominated by a phase whose equation of state is stiffer than radiation. Kination is a regime where the kinetic energy of a scalar field is dominant against its potential energy. In the limiting case $w = 1$, where the sound velocity is equal to the speed of light, the energy density of the stiff fluid scales as $\rho \sim a^{-6}$. Such a scenario is natural in theories with runaway potentials, e.g. theories with moduli fields.

We examine the kination scenario because it has striking implications both for the PBH formation and the IGW produced. Our numerical results complement previous studies [42] and we show that an early universe kination domination (eKD) era shapes in a different way the spectrum of the tensor perturbations. This fact renders the eKD era testable.

We comment that the attribute "early" to kination might sound redundant since there is no kination era observed in the universe. Nevertheless we use it to emphasize that the kination era assumed precedes the standard radiation era.

The redshift of the stiff fluid energy density is the fastest and any ambient radiation will sooner or latter dominate the early universe. Hence, a kination era ends

naturally if there is an extra fluid with softer equation of state. Besides this gradual transition, an eKD era can end suddenly. The later is simpler to examine because the scalar transfer function can be computed explicitly due to the discrete w values and single fluid analysis.³

Let us consider an early kination domination scenario that transits suddenly into the RD phase. The transition takes place at the reheating temperature T_{rh} . The transfer function in the kination domination cannot be written in closed analytical expressions. One can only rely on approximate methods, since the Bessel functions of order one involved can only be written as infinite series and not further simplified. Hence, we treat the scenario eKD to RD numerically. Further, in order to simplify our calculations we utilize a monochromatic power spectrum of scalar perturbations modeled by a delta distribution peaked at k_p , given by Eq. (20). Such a choice models a narrow and sharply peaked $\mathcal{P}_{\mathcal{R}}$. In the conclusions, we will discuss a correspondence between δ -type and Gaussian distributions, and anticipate features for the IGWs produced by a wider $\mathcal{P}_{\mathcal{R}}(k)$.

In a sudden eKD \rightarrow RD scenario, the scale factor is a piecewise defined function, that is continuous at the point of transition $\eta = \eta_{\text{rh}}$,

$$a(\eta) = \begin{cases} \sqrt{\frac{\eta}{\eta_{\text{rh}}}}, & \eta < \eta_{\text{rh}} \\ \frac{\eta + \eta_{\text{rh}}}{2\eta_{\text{rh}}}, & \eta \geq \eta_{\text{rh}} \end{cases} \quad (22)$$

A similar expression can be obtained for the conformal Hubble parameter, \mathcal{H} . The scalar transfer function, Eq. (2), is given by

$$\Phi(x) = \begin{cases} \frac{2}{x} J_1(x), & x < x_{\text{rh}} \\ \frac{3}{x^2} \left[C_1 \left(\frac{\sin(x/\sqrt{3})}{x/\sqrt{3}} - \cos(x/\sqrt{3}) \right) + C_2 \left(\frac{\cos(x/\sqrt{3})}{x/\sqrt{3}} + \sin(x/\sqrt{3}) \right) \right], & x \geq x_{\text{rh}} \end{cases} \quad (23)$$

After the transition, into the RD era, we write the solution to Eq. (2) as a linear combination of $(x/\sqrt{3})^{3/2} \cdot J_{3/2}(x/\sqrt{3})$ and $(x/\sqrt{3})^{3/2} \cdot Y_{3/2}(x/\sqrt{3})$ with two constant coefficients C_1 and C_2 . We determine the C_1 and C_2 by the continuity of the potential and its derivative at the point of the transition, after expressing $J_{3/2}$ and $Y_{3/2}$ in terms of spherical Bessel functions. The plot of the absolute value of Eq. (23) is depicted in Fig. 1. The $\Phi(x)$ remains constant as long as $x \ll 1$. At the horizon

crossing, $\eta = \eta_{\text{entry}}$, the gravitational potential starts decaying as Eq. (23) dictates: roughly as $x^{-3/2}$ during eKD and after the transition to the RD phase, as x^{-2} .

The reheating conformal time η_{rh} is inversely proportional to the reheating temperature, $\eta_{\text{rh}} \propto T_{\text{rh}}^{-1}$. This means that higher reheating temperature scenarios predict a faster reheating transition into RD. During eKD the growth of IGWs goes proportional to conformal time for a given wave mode k ; i.e., $\Omega_{\text{IGW}}^{(\text{KD})} \sim (k_p \eta)^2 \bar{I}_{\text{KD}}^2 \propto \eta \propto a^2$. This growth stalls once the transition is completed and radiation takes over. In the cases that $\eta_{\text{entry}} \ll \eta_{\text{rh}}$, we neglect the effect from RD era, because by that time the gravitational potential sourcing the tensor modes is negligibly small. Numerically, in those cases we calculate

³ A mechanism that can implement a sudden transition can be easily conceived: an extra field direction that ends the kination stage via a waterfall transition to a global minimum where the field decays and reheats the universe.

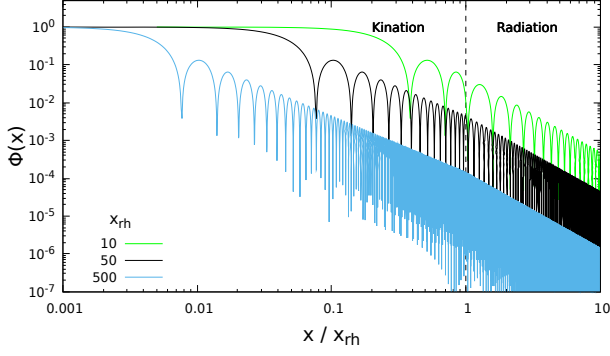


FIG. 1. The transfer function in the case of the eKD→RD sudden transition in the Newtonian gauge. We plot the absolute value of the gravitational potential, Eq. (23), for $x_{\text{rh}} = 10, 50, 100$. The horizontal axis is normalized so that the transition occurs at 1.

the IGWs at the time of transition⁴. Therefore, sudden eKD to RD scenarios may show up in the experiments with an enhanced IGW spectrum.

When there is a fast reheating, i.e., right after the horizon entry of the perturbation the universe transits into the radiation regime, the growth, $\Omega_{\text{IGW}} \propto a^2$, of IGWs ceases early. However, the gravitational potential has not been suppressed significantly, and the contribution from RD era is important. In such a case of fast reheating we calculate the IGWs at a conformal time $\eta_c = 50 \eta_{\text{rh}} \gg \eta_{\text{rh}}$, thus taking into account the non-negligible contribution from the RD era. In Fig. 2, we present the evolution of the time-dependent piece of the IGW spectral shape with respect to the conformal time for the transition eKD→RD.

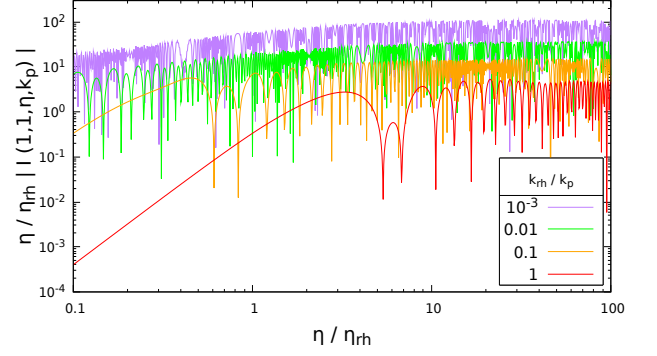


FIG. 2. The behavior of the time-dependent piece of the IGW spectrum under a sudden eKD→RD transition. The transition occurs when $\eta/\eta_{\text{rh}} = 1$. Here we plot the combination $(\eta/\eta_{\text{rh}}) |I|$ for $k_{\text{p}}/k = 1$ and for four choices of the ratio $k_{\text{rh}}/k_{\text{p}}$ corresponding to different colors in this figure. The growth is proportional to $\sqrt{\eta}$ during eKD. After the transition, this function always approaches an oscillatory state with a constant amplitude in the late times.

The final formula for the density parameter of IGWs in the eKD→RD transition is given by

$$\Omega_{\text{IGW}}^{\text{eKD} \rightarrow \text{RD}}(\eta_c, k) = \frac{1}{6} A_{\mathcal{R}}^2 \left(\frac{k_{\text{p}}}{\mathcal{H}(\eta_c)} \right)^2 \left[1 - \left(\frac{k}{2k_{\text{p}}} \right)^2 \right]^2 \times \overline{I_{\text{eKD} \rightarrow \text{RD}}^2 \left(\frac{k_{\text{p}}}{k}, \frac{k_{\text{p}}}{k}, \eta_c, k \right)} \Theta \left(1 - \frac{k}{2k_{\text{p}}} \right). \quad (24)$$

Here the unit step function Θ is included by conservation of momentum, so that tensor modes with $k > 2k_{\text{p}}$ are cut off. We remind the reader that we have assumed a delta-type power spectrum for the curvature perturbation. Later, in our results in Sec. V and conclusions in Sec. VI, we estimate the amplitude of the Ω_{IGW} for a broad curvature power spectrum, of Gaussian type, at the peak frequency.

Finally, let us mention that the existence of an early kination phase implies that the energy density of the produced IGW gets enhanced and might backreact on the geometry. This backreaction must be limited in order that the energy density of the IGWs during the BBN does not increase the expansion rate to a disturbing level for the observed abundances of the relic nuclei. In order to comply with this constraint we find out a new bound on the reheating temperature that must be satisfied,

$$T_{\text{rh}} \gtrsim 10^7 \text{ GeV } A_{\mathcal{R}}^{3/2} \left(\frac{M/\gamma}{10^{20} \text{ g}} \right)^{-1/2}. \quad (25)$$

This is a rough, conservative bound that connects horizon mass M/γ and the $A_{\mathcal{R}}$ with the T_{rh} , and guarantees the success of the BBN predictions. Further discussion and derivation details can be found in Appendix A.

⁴ After the transition, a sharp peak appears at $k = \frac{2}{\sqrt{3}} k_{\text{p}}$ superimposed on the spectral shape obtained at $\eta = \eta_{\text{rh}}$. This corresponds to a logarithmic divergence manifest in the radiation domination as can be seen in Eq. (21). We neglect such a resonance peak as it has no physical meaning, but it is rather a mathematical singularity associated to the delta power spectrum we used, Eq. (20)

IV. PRIMORDIAL BLACK HOLES AND THE ASSOCIATED GRAVITATIONAL WAVE SIGNAL

PBHs form from the collapse of large-amplitude primordial inhomogeneities [62–65]. An inhomogeneity decouples from the background expansion if the power spectrum $\mathcal{P}_{\mathcal{R}}(k)$ is enhanced at a scale k^{-1} , characteristic of the PBH mass. During RD, typical values for the $\mathcal{P}_{\mathcal{R}}(k) \sim \mathcal{O}(10^{-2})$ are required. If PBHs have mass $M < 10^{15}$ g evaporates at time scales less than the age of the universe, whereas PBHs with $M > 10^{15}$ g survive till today being dynamically cold component of the dark matter in galactic structures.

The PBH dark matter scenario is constrained in a wide range for the mass parameter M by several observational experiments, labeled with extra galactic gamma-ray background (EGB), V, GC, HSC, O, EM, LIGO/VIRGO, GW2, supernova (SN), wide binaries (WB), E, x-ray binaries (XB), Planck (PA) in Fig. 6. In the present universe, the abundance of light PBH is constrained from the extra galactic gamma-ray background [66–70], as well as from positron constraints (V) [71]. Black holes of mass above 10^{17} g are subject to gravitational lensing constraints [72–74], given by Subaru (HSC), Ogle (O), EROS (E), and MACHO (M), microlensing of SN and others. The CMB anisotropies measured by PA constrains the PBH with mass above 10^{33} g [75–80]. At the large mass region there are also constraints from accretion limits in X-ray and radio observations [81] and XB [16]. There are also dynamical limits from disruption of WB, survival of star clusters in Eridanus II. Second order tensor perturbations (GW2) generated by scalar perturbations already constrain the abundance of PBH masses approximately in the range $10^{30} - 10^{33}$ g. Also, the expected GWs generated by PBH binaries with mass $\mathcal{O}(1 - 10)M_{\odot}$ coalescing at the present epoch is constrained by LIGO/Virgo [82–84] as well as compact binary systems with component masses in the range $0.2 - 1M_{\odot}$ [85] shown in Fig. 6. For a recent update on the PBH constraints see Ref. [16].

A. PBH abundance for general EOS

The present relic energy density parameter of primordial black holes with mass M produced at the cosmic time t is

$$\Omega_{\text{PBH}}(M) = \Omega_{\text{m}} \gamma \beta(M) \left(\frac{M_{\text{rh}}}{M/\gamma} \right)^{\frac{2w}{1+w}} \left(\frac{M_{\text{eq}}}{M_{\text{rh}}} \right)^{1/2} \tilde{g}(g_*) \quad (26)$$

where $\tilde{g}(g_*) = 2^{1/4} (g_*(t)/g_*(t_{\text{rh}}))^{-s/4} (g_*(t_{\text{rh}})/g_*(t_{\text{eq}}))^{-1/4}$ and g_* the thermalized degrees of freedom. The parameter s is equal to 1 for $t > t_{\text{rh}}$ and 0 for $t < t_{\text{rh}}$. Ω_{m} is the total matter density parameter today, M_{eq} is the horizon mass at the moment of matter radiation equality, and M_{rh} the horizon mass at the moment of reheating.

The $\beta(M)$ is the mass fraction of the universe with horizon mass M/γ that collapsed and formed PBHs; it

can be interpreted as the black hole formation probability. Assuming Gaussian statistics, for a spherically symmetric region it is

$$\beta(M) = \int_{\delta_c} d\delta \frac{1}{\sqrt{2\pi\sigma^2(M)}} e^{-\frac{\delta^2}{2\sigma^2(M)}}, \quad (27)$$

where $\sigma(M)$ is the variance of the density perturbations and δ the density contrast. The PBH abundance has an exponential sensitivity to the variance of the perturbations $\sigma(M)$ and the threshold value δ_c , which is w dependent. In this work, we assign values to δ_c following the findings of Ref. [86].

The horizon mass increases with a different rate for different expansion rates. Using the relation $f = k/(2\pi)$ we find the frequency-PBH mass correspondence for general equation of state w and reheating temperature T_{rh} ,

$$f_{\text{hor}}(M, T_{\text{rh}}, w) \simeq 2.7 \times 10^2 \text{Hz} \left(\frac{T_{\text{rh}}}{10^{10} \text{GeV}} \right)^{\frac{1-3w}{3(1+w)}} \left(\frac{M/\gamma}{10^{12} \text{g}} \right)^{-\frac{3w+1}{3(1+w)}} \left(\frac{g_*}{106.75} \right)^{-\frac{2w}{6(1+w)}}. \quad (28)$$

In the above relation,⁵ we have assumed a one-to-one correspondence between k (or f) and the PBH mass M . This is true for the approximation of a monochromatic PBH mass spectrum, which is practically the case in many models. We note that the PBH mass distribution peaks at a value $M(k)$ that is in a slight offset with the value $M(k_{\text{p}})$, as our following numerical analysis shows. In the k -space the peak of the $\sigma(k)$ is about at $0.7k_{\text{p}}$ [31]. The $f(M, T_{\text{rh}}, w)$ relation is depicted in Fig. 3. The $f_{\text{hor}}(M)$ frequency and $f_{\text{p,IGW}}$ frequency, where the IGW spectrum maximizes, have similar size but do not coincide.

Therefore, searching for GWs with frequency f_{IGW} , one can probe PBH scenarios and the reheating temperature of the universe.

B. GW detectors and PBH scenarios

Currently, there is a network of operating ground-based GW detectors that focus on the high and low frequency regime, roughly at 10^2 and 10^{-9} Hz, of the GW spectrum. Additionally, there are several designed and proposed experiments sensitive enough to detect or constrain the stochastic GW background at a large range of frequencies. In this subsection, we outline the GW experiments labeled in Fig. 5 that can test the predictions of the models described in this work.

⁵ For the case of kination domination the minor correction of replacing T_{rh} by $2^{1/4}T_{\text{rh}}$ should be considered if there is equipartition between radiation and scalar field energy density at the time of reheating.

The operating ground-based GW detector system is the advanced Laser Interferometer Gravitational wave Observatory (aLIGO). In Fig. 5 we show for reference O1 and O5 which correspond to the first observing run and the design sensitivity respectively [87]. The future ground-based laser third generation interferometers is the Einstein Telescope (ET) [88], that probes the range of frequencies near 100 Hz. The space-based proposed experiments are DECIGO [89, 90] and BBO [91], that will probe in the decihertz frequency window. In the millihertz band of the spectrum there is the scheduled LISA, [92], and proposed space-based experiments such as the TianQin, [93]. Pulsar Timing Arrays, with the international PTA (IPTA) [94], and the planned Square Kilometer Array (SKA) [95] are projects that probe and already pose constraints on the nanohertz regime.

Fitting functions regarding the sensitivity curves for LISA, aLIGO and ET are provided by [96]; for DECIGO and BBO, we consulted [97] and adjusted the sensitivities of these experiments to current values and expectations; for TianQin, we used the fitting function provided in Ref. [98].

IGWs can constrain a large window of the PBHs masses. Currently, there are indirect constraints from the pulsar timing array experiments on IGWs associated with the formation of relatively massive PBHs at the epoch of horizon entry. Notably, a very severe constraint exists, $\beta(M) \lesssim 10^{-52}$, in the solar mass range, from pulsar timing data [13, 99]. We note that Ref. [100] pointed out that the tension with PTA constraints can be relieved if the perturbations are locally non-Gaussian.

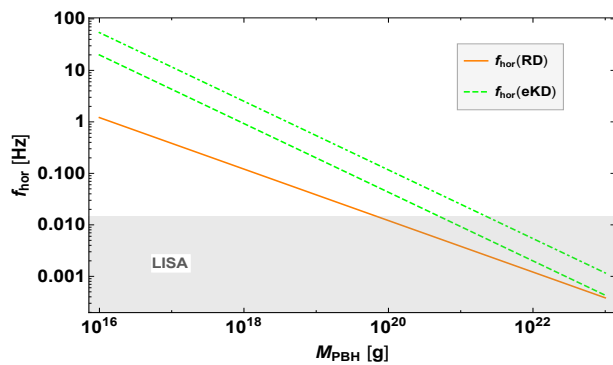


FIG. 3. The figure depicts the relation between the PBH mass M_{PBH} and the corresponding frequency of horizon with size $k^{-1} = (2\pi f_{\text{hor}})^{-1}$ and mass M_{PBH}/γ for two equation of states $w = 1/3$ (orange line) and $w = 1$ (green lines); see Eq. (28). The reheating temperature is $T_{\text{rh}} = 10^4$ GeV (5×10^2 GeV) for the dashed (dot-dashed) lines. The gray strip highlights the frequency band of LISA optimal sensitivity.

V. RESULTS

In this section we outline our findings. We assume $\mathcal{P}_{\mathcal{R}}(k)$ amplitudes and wave numbers having as a ruler the PBH abundance, and then we calculate IGWs aiming at constraining early universe cosmological scenarios and inflationary models.

We consider $\mathcal{P}_{\mathcal{R}}(k)$ peaks generated by the α -attractors [48] and nonminimal derivative coupling Horndeski inflation [50], as well as, irrespectively of the inflationary theory, Gaussian and Dirac δ -type distributions. The peak choice of the $\mathcal{P}_{\mathcal{R}}$ is spanning a wide range of frequencies in the GW spectrum; see Fig. 4. We compare the resulting IGW shape with the sensitivity of current, planned and proposed GW experiments. We choose amplitudes and shapes for the $\mathcal{P}_{\mathcal{R}}(k)$ that induce GWs and PBH abundances of cosmologically significant amount. We always make sure that our input parameters respect the current constraints for the PBH abundance and the GWs. We also take care the position and the width of the $\mathcal{P}_{\mathcal{R}}(k)$ peak to respect constraints coming from the Hawking radiation [14].

We assemble and present our results considering first $\mathcal{P}_{\mathcal{R}}(k)$ that generate a sizable amount of both PBHs and IGWs and secondly $\mathcal{P}_{\mathcal{R}}(k)$ that generate only IGWs with the PBH counterpart being either negligibly small, $\Omega_{\text{PBH}} \lesssim 10^{-10}$, or promptly evaporating.

A. IGWs in scenarios with dominant and subdominant PBH dark matter component

1. Significant PBH abundance

In the mass window $M = 10^{17} - 5 \times 10^{22}$ g, the PBH abundance can reach its maximum value,⁶ $\Omega_{\text{PBH}}/\Omega_{\text{DM}} = 1$; see Ref. [16]. If PBHs constitute a significant fraction of the total dark matter then an IGW counterpart must exist that can be tested by LISA and by proposed experiments such as BBO and DECIGO.

Another motivated PBH mass range is $M = \mathcal{O}(1 - 100)M_{\odot}$ where LIGO detected several coalescence events the last years with the most recently published the intriguing event [107]. For that PBH mass range the IGWs are expected to produce GWs with nanohertz frequency detectable by PTA experiments [99].

The exact PBH mass parameters that we choose can be found in Tables II and III and in Fig. 6. In the tables, the order of magnitude value for PBH abundance is quoted due to the exponential sensitivity to the model-dependent threshold value δ_c .

⁶ In that range there are feeble constraints coming from white dwarfs and neutron stars [101–104] but these constraints, together with others in the same mass range such as femtolensing and picolensing, are seen as insecure [16, 105, 106].

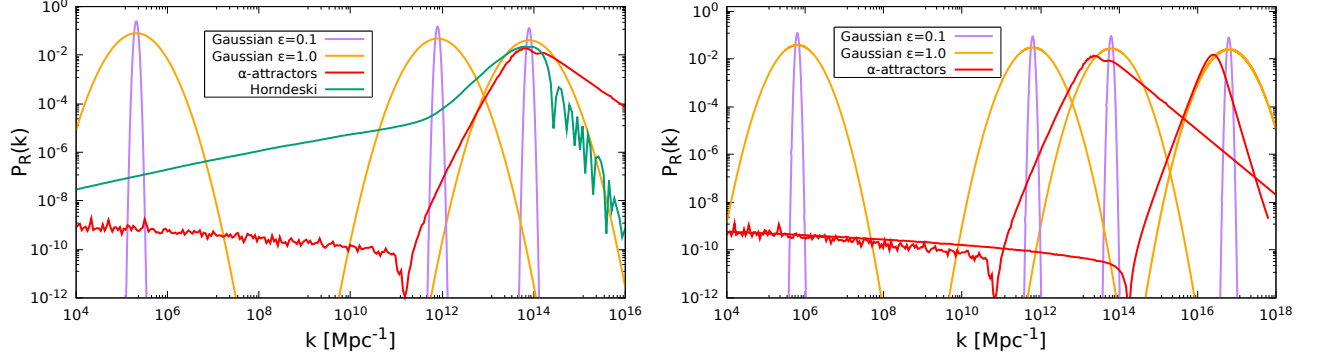


FIG. 4. The power spectra of curvature perturbations sourcing IGWs during RD. We consider a medium and a narrow Gaussian shapes for $\mathcal{P}_{\mathcal{R}}(k)$ as well as $\mathcal{P}_{\mathcal{R}}(k)$ produced by α -attractors (red curves) and Horndeski nonminimal derivative coupling inflation models (green curve). The scaling of each $\mathcal{P}_{\mathcal{R}}(k)$ slope is given in Table I. Oscillations in the red curves correspond to numerical effects. *Left panel:* $\mathcal{P}_{\mathcal{R}}(k)$ that generates significant PBH abundances, $\Omega_{\text{PBH}} \sim \mathcal{O}(0.01 - 1)$. *Right panel:* $\mathcal{P}_{\mathcal{R}}(k)$ that generates negligible PBH abundances, $\Omega_{\text{PBH}} \lesssim 10^{-10}$.

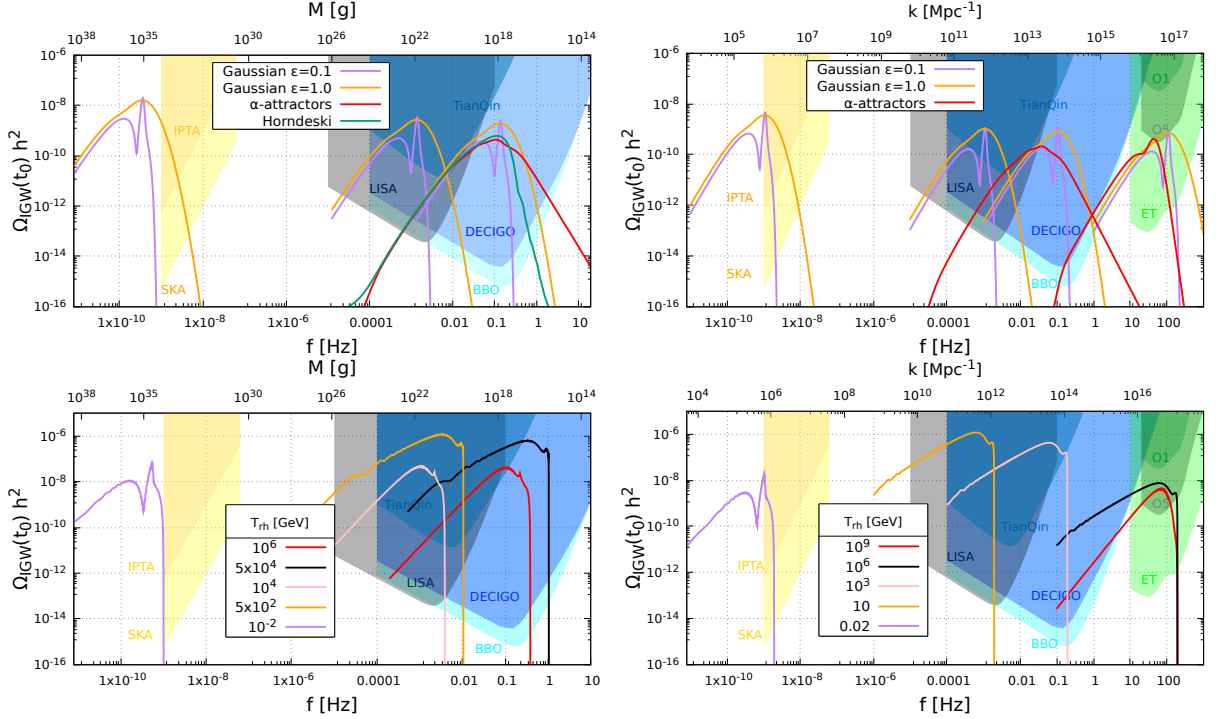


FIG. 5. The IGW spectral shapes for two early universe scenarios, the RD (*top panels*) and the eKD \rightarrow RD (*bottom panels*) sourced by $\mathcal{P}_{\mathcal{R}}(k)$ depicted in Fig. 4. In the *left panels* we consider the scenario of abundant PBH production and in the *right panels* negligible PBH abundances. In the background of the IGW spectral curves the sensitivity curves of current/planned/proposed GW detectors are shown as described in the subsection IV B. The parameters for the $\mathcal{P}_{\mathcal{R}}(k)$ and the derived values for the IGWs are listed in the Tables II-V.

2. Negligible PBH abundance

Contrary to the exponential sensitivity of the Ω_{PBH} on the $A_{\mathcal{R}}$, the sensitivity of the IGWs amplitude on the $A_{\mathcal{R}}$ is of a power-law type. Therefore, a minute decrease in the $\mathcal{P}_{\mathcal{R}}(k)$ amplitude can nearly disappear the PBHs abundance while decrease the IGW amplitude only by a minor amount. This is rather fascinating because pri-

mordial density perturbations washed out completely by the RD era have left a relic GW behind that reveals their presence.

In addition, there are PBH masses that evaporate promptly in the early universe. These PBHs do not survive until today and, unless a stable remnant is left behind, the corresponding Ω_{PBH} is zero and cannot account for the dark matter in the galaxies. Nevertheless, the as-

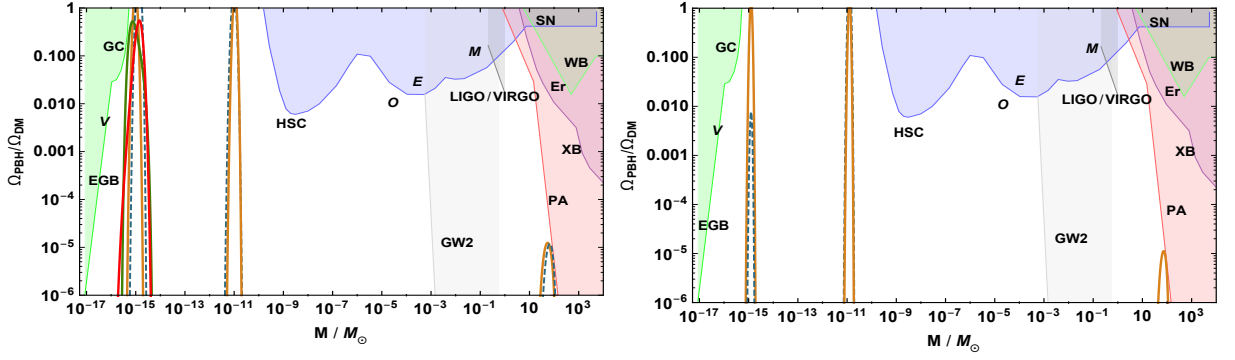


FIG. 6. The fractional abundance of the PBHs produced during RD (left panel) and eKD (right panel) for our $\mathcal{P}_{\mathcal{R}}(k)$ scenarios. The colored upper bounds are the present experimental constraints as described in Sec. IV. In the left panel, the red curve corresponds to the α -attractor inflationary model, the green to the Horndeski nonminimal derivative coupling model, the orange to a Gaussian of width $\epsilon = 1$, and the dashed to a Gaussian of width $\epsilon = 0.1$. The $\mathcal{P}_{\mathcal{R}}(k)$ for each curve is depicted in Fig. 4. In the right panel, we take a δ -distribution for the $\mathcal{P}_{\mathcal{R}}$; also, for the orange curves the reheating temperature is higher than for the dashed curves. Detailed values can be found in Tables II and III, respectively; the associated IGWs are depicted in Fig. 5. M_\odot stands for the sun mass, roughly 2×10^{33} g.

sociated IGWs might be strong enough to be detectable. Such a possibility is rather interesting because the PBH remnants can constitute a significant fraction of the total Ω_{DM} and, moreover, the inflationary scenarios that predict mini-PBHs can have a spectral index n_s in full accordance with the Planck-2018 data [49], see Eq. (B3) for the α -attractors potential that we use.

Our results for zero or negligible PBH abundance are listed in Tables IV and V. We note that, instead of Ω_{PBH} , we write the $\beta(M)$ values, see Eq. (27), since PBH with mass $M \lesssim 10^{15}$ g has already evaporated.

B. Cosmological eras

1. Radiation

The spectral shapes of the IGWs produced during the radiation era are depicted in the upper panels of Fig. 5. For narrow Gaussian $\mathcal{P}_{\mathcal{R}}(k)$ peaks, $\epsilon = 0.1$, the spectral shape obtained has a double peak structure with a sharp peak at $f \simeq 2f_p/\sqrt{3}$, resembling the IGW spectrum generated by a δ -distribution for $\mathcal{P}_{\mathcal{R}}(k)$. For a broader $\mathcal{P}_{\mathcal{R}}(k)$ peak a single wide peak forms in the IGWs at approximately $2f_p/\sqrt{3}$, see top panels of Fig. 5.

The α -attractor inflationary model, described by the potential (B2), generates an enhanced $\mathcal{P}_{\mathcal{R}}(k)$ as depicted in Fig. 4. The predicted IGW spectrum resembles more that of the broad Gaussian, $\epsilon = 1$, with a peak shifted towards k_p , i.e. $f_{p,\text{IGW}} \simeq f_p$. The general nonminimal derivative coupling model, see Eqs. (18), (B4) and (B5), features an IGW spectrum that resembles the broad Gaussian; hence it also resembles the α -attractor model around the peak. However, the IGW spectra of the two inflationary models deviate at large frequencies following the different scaling at the high- k tale of the $\mathcal{P}_{\mathcal{R}}(k)$, as the inspection of Figs. 4 and 5 shows.

For the case the $A_{\mathcal{R}}$ amplitude is decreased to a level that the PBH abundance becomes negligible, $\Omega_{\text{PBH}} \lesssim 10^{-10}$, the amplitude of the IGWs decreases a little and the spectral shape characteristics remain unchanged. For the case of evaporating mini-PBHs, we examine a different α -attractors model, described by the potential (B3). This model generates a $\mathcal{P}_{\mathcal{R}}(k)$ peak that is relatively narrow. The spectrum of the IGWs is found to feature a double peak structure, manifest in the Figs. 4 and 5.

Regarding the energy density, we find that the growth of the IGWs amplitude occurs rapidly, for a period $\eta_c \sim O(10)k_p^{-1}$, and then the growth ceases. The growth is realized from the time of entry until the potential decreases significantly, since $\Phi(x)$ oscillates with a x^{-2} decaying amplitude in subhorizon scales. Afterward the source term becomes negligible and the GW propagates freely. At that time η_c the Ω_{IGW} produced by a Gaussian $\mathcal{P}_{\mathcal{R}}(k)$ peak with width ϵ and at the frequency f_p is

$$\Omega_{\text{IGW}}^{(\text{RD})}(\eta_c, f_p) \sim (A_{\mathcal{R}} \epsilon \sqrt{\pi})^2. \quad (29)$$

A similar relation has been found following analytic steps in Ref. [52]. We further comment on the scaling of the IGW spectrum, at scales beyond the peak, in the next subsection. Note that in Tables II-V the present total energy density value, $\Omega_{\text{IGW}}(t_0) = \int d \ln f \Omega_{\text{IGW}}(t_0, f)$, is listed.

2. Early kination

The IGWs produced during the early kination era and sourced by δ -distributions for $\mathcal{P}_{\mathcal{R}}(k)$ are depicted in the lower panels of Fig. 5. The increase of the IGW amplitude is depicted in Fig. 2. What is of interest is that the shape of the IGW spectrum depends on the reheating temperature, always assuming a sudden change from eKD to RD at the temperature T_{rh} .

If the δ peak enters well before the reheating moment, $\eta_{\text{entry}} \ll \eta_{\text{rh}}$, the induced tensor power spectrum has a distinctive shape, characteristic of the kination stage. It is distinctive because the scalar perturbations decay as $x^{3/2}$ experiencing a maximal pressure. No sharp peak in the IGWs appears even for the monochromatic $\mathcal{P}_{\mathcal{R}}(k)$. This feature has been also noted in [42]. Additionally, the energy density of the IGWs gets enhanced due to the redshift of the stiffer background. We call this transition "slow eKD \rightarrow RD."

If, on the other hand, the reheating happens fast after the horizon entry of the δ -peak, the scalar perturbations experience the maximal pressure of the stiff fluid only for a while. It is actually the radiation phase that mostly forms the IGW spectrum. We call this transition "fast eKD \rightarrow RD". This is readily seen at the IGW spectrum in the PTA frequency range, as depicted in Fig. 5, where the BBN bound for the T_{rh} limits the duration of the kination era. The parameters chosen for this case are $k_{\text{p}}\eta_{\text{rh}} \approx 1.5$ which means that transition essentially occurs at the moment of entry of the curvature perturbation. Apparently, the distinction between the pure RD and the very fast eKD \rightarrow RD transition is hard to be made. By decreasing the η_{entry} , the differences in the amplitude and the f -scaling become manifest.

We note that, in our examples, the amplitude A_0 for the δ -distribution together with the T_{rh} value has been chosen so that either the Ω_{PBH} or the Ω_{IGW} is maximized, given the observational constraints. Thus, these eKD scenarios can be probed in the near future by gravitational wave observatories. Also, a change in the T_{rh} , apart from uplifting/downlifting the Ω_{IGW} shifts the position of the spectrum changing the frequency $f_{\text{p,IGW}}$.

Regarding the energy density, the IGWs at the time η_c in the radiation era have an energy density parameter

$$\Omega_{\text{IGW}}^{(\text{KD})}(\eta_c) \approx \frac{\eta_{\text{rh}}}{\eta_{\text{entry}}} A_0^2. \quad (30)$$

This result is found for a monochromatic scalar power spectrum. Utilizing the correspondence between the δ and the Gaussian distribution with width ϵ ,

$$A_0 \longleftrightarrow A_{\mathcal{R}} \equiv \frac{A_0}{\epsilon\sqrt{\pi}}, \quad (31)$$

one can find the energy density parameter of the IGWs produced during the kination era for wide $\mathcal{P}_{\mathcal{R}}(k)$ distributions as well.

C. Fitting broken power laws for IGW spectra

In this subsection we make a few notes on the power laws that describe the IGW spectral curves in Fig. 5, and facilitate the detectability of our results. The power laws for each case are listed in Table I together with the power-law scaling of the "mother" curvature power spectrum. We separately describe the scaling in the IR part of the

spectrum for $f < f_{\text{p,IGW}}$ and in the UV part for $f > f_{\text{p,IGW}}$. For a recent independent investigation regarding the infrared scaling of the IGWs spectra see also [51], and [1] for a broken power law analysis for general stochastic GW backgrounds.

- The Gaussian models produce IGWs that scale as a power law f^3 for $f < f_{\text{p,IGW}}$, despite that the Gaussian $\mathcal{P}_{\mathcal{R}}(k)$ demonstrates very steep slopes such as k^8 ($\epsilon = 1$) or k^{40} ($\epsilon = 0.1$), estimated at about the half of the curve's peak height. In the UV frequency band, $f > f_{\text{p,IGW}}$, the $\epsilon = 0.1$ Gaussian is almost cut off whereas the $\epsilon = 1$ falls off roughly as f^{-10} .
- The first α -attractors inflationary model, given by Eq. (B2), produces a $\mathcal{P}_{\mathcal{R}}(k)$ that increases like k^4 in the beginning, like k^3 before the peak and then falls like $k^{-1.2}$. The spectrum of the IGWs scales mainly f^3 in the IR frequencies, similarly to the power-law scaling of the GNMDC model. In the UV it scales like a $f^{-2.7}$. The IGW spectrum is found to be broader.
- The second α -attractors inflationary model, given by Eq. (B3), triggers evaporating mini-PBH formations and induced GWs near the LIGO frequency band. The produced $\mathcal{P}_{\mathcal{R}}(k)$ increases like k^4 and falls like k^{-4} . The associated IGWs scale like f^3 in the IR band and like f^{-9} in the UV band.
- The Horndeski general nonminimal derivative coupling (GNMC) inflation model produces a $\mathcal{P}_{\mathcal{R}}(k)$ that scales like $k^{2/5}$ at small wave numbers, after like k^2 and then falls like k^{-4} . The IGW spectrum has mainly a f^3 scaling in the IR band and f^{-7} power law scaling in the UV.

Apparently, the distinction between α -attractors and the Horndeski GNMDC inflationary models can be made in the large- f region.

- For the eKD case, the scaling of IGWs follows a power-law behavior, proportional to f in the IR band. The UV part drops abruptly, consistent with our choice of delta distribution for $\mathcal{P}_{\mathcal{R}}$. In the case of a fast transition into RD, the scaling, as expected, goes like f^2 in the IR.

We summarize the scaling for IGWs in Table I.

In the IR band, as a general rule, GWs induced during the radiation era have a spectrum that follows a f^3 power law under for a broad $\mathcal{P}_{\mathcal{R}}$ and a f^2 power-law for a monochromatic $\mathcal{P}_{\mathcal{R}}$.⁷ Our result agrees with the conclusions of [51] as well as with the GW spectrum described

⁷ We comment that our IGW spectra are found to be broad enough and are not expected to experience a deformation, mentioned recently in [108], via the Sachs-Wolfe and integrated Sachs-Wolfe effect as the GWs travel toward the detectors.

era	$\mathcal{P}_{\mathcal{R}}(k)$	k_{IR}	k_{UV}	f_{IR}	f_{UV}
RD	Gauss. #1			f^3	cut-off
	Gauss. #2			f^3	f^{-10}
	α -attr. #1	k^4, k^3	$k^{-1.2}$	f^3	$f^{-2.7}$
	α -attr. #2	k^4	k^{-4}	f^3	f^{-9}
	GNMDC	$k^{2/5}, k^2$	k^{-4}	f^3	f^{-7}
	δ	-	-	f^2	cut-off
fast eKD	δ	-	-	f^2	cut-off
slow eKD	δ	-	-	f	cut-off

TABLE I. We list the approximate power-law scaling that describes the IGW spectral shapes for the $\mathcal{P}_{\mathcal{R}}(k)$ models we studied, from IR to UV bands. k_{IR} (k_{UV}) represents the wave numbers $k < k_{\text{p}}$ ($k > k_{\text{p}}$), and f_{IR} (f_{UV}) the frequencies $f < f_{\text{p,IGW}}$ ($f > f_{\text{p,IGW}}$). The "cutoff" means that the IGW spectrum falls off very abruptly in the UV. The Gauss. #1 and Gauss. #2 models stand for the narrow and medium width Gaussians $\epsilon = 0.1$, $\epsilon = 1$, respectively. The α -attr. #1 and α -attr. #2 stand for the α -attractors inflation models with potentials (B2) and (B3), respectively.

in [52].⁸ In the slow eKD→RD scenario, where most of the GWs are induced during the kination era, the spectrum increases as f in IR frequency band.

In the UV frequency band, for almost all cases, the spectrum falls off very abruptly and it is cutoff in the monochromatic cases. The exception is the first α -attractors inflation model (B2) that features a broader $\mathcal{P}_{\mathcal{R}}(k)$ that falls off slowly, $\mathcal{P}_{\mathcal{R}}(k) \sim k^{-1.2}$. Hence, broad scalar power spectra can be distinguished from the narrow ones via the spectrum of the induced GWs.

VI. CONCLUSIONS

In this work we have explored the features of the scalar-induced GW spectrum produced by different types of $\mathcal{P}_{\mathcal{R}}(k)$ peaks and for two different early universe cosmological scenarios: radiation and kination domination. In addition, we examined two explicit inflationary models that generate PBHs, α -attractors, and Horndeski general nonminimal derivative coupling models, and tested the predicted IGW signals against the observational constraints.

Assuming a Gaussian $\mathcal{P}_{\mathcal{R}}(k)$ with amplitude $A_{\mathcal{R}}$ and width ϵ we find that the IGWs produced during radiation era have a spectral energy density parameter today, at the frequency f_{p} where the $\mathcal{P}_{\mathcal{R}}$ maximizes, given by

$$\Omega_{\text{IGW}}^{(\text{RD})}(t_0, f_{\text{p}}) \sim 5.2 \times 10^{-9} \epsilon^2 \left(\frac{g_*}{106.75} \right)^{-1/3} \left(\frac{A_{\mathcal{R}}}{10^{-2}} \right)^2. \quad (32)$$

For IGWs produced during kination domination, with T_{rh} the reheating temperature, the corresponding expression

for the energy density today is

$$\Omega_{\text{IGW}}^{(\text{KD})}(t_0, f_{\text{p}}) \sim \pi \Omega_{\text{IGW}}^{(\text{RD})}(t_0, f_{\text{p}}) \left(\frac{10^7 \text{ GeV}}{T_{\text{rh}}} \right) \left(\frac{f_{\text{p}}}{\text{Hz}} \right) \quad (33)$$

where $\Omega_{\text{IGW}}^{(\text{RD})}(t_0, f_{\text{p}})$ is given by Eq. (32).

The RD and an eKD era may be distinguished by their power-law scaling in the small- f band, $f < f_{\text{p,IGW}}$. An eKD scenario with a slow reheating and sudden transition to RD predicts spectral shapes with large amplitudes for IGWs. Over the next years, aLIGO, reaching its design sensitivity, will put constraints on the eKD scenario in the high frequency band of the spectrum. Hints for the reheating temperature can be found if the IGW spectrum has been modified due to the transition into the radiation era.

A calculation involving a δ -distribution is simpler to implement, compared to the Gaussian or any other realistic distribution such as those of α -attractors, since the integrals (11) can be computed analytically. We used δ , i.e. monochromatic, distributions only for the eKD case, because a broad distribution is computationally more costly in that case. Utilizing the correspondence, Eq. (31), between δ and Gaussian distributions, $A_0 \longleftrightarrow A_{\mathcal{R}}$, the maximum Ω_{IGW} can be found following analytic steps and in a good approximation, either for the RD or the eKD case.

The spectral shape for the $\Omega_{\text{IGW}}(t_0, f)$ depends on the features of the source, the scalar spectrum $\mathcal{P}_{\mathcal{R}}(k)$. It maximizes at a frequency $f_{\text{p,IGW}}$, in a little offset from f_{p} , depending on the width of the $\mathcal{P}_{\mathcal{R}}(k)$, as the results listed in the Tables IV and V demonstrate. Although the power-law scaling of the IGWs increases roughly universally as f^3 for RD, it falls off with different scaling. It is interesting to mention that, for the radiation domination case at least, the $\mathcal{P}_{\mathcal{R}}(k)$ shape is projected in a much more informative manner onto the $\Omega_{\text{IGW}}(f)$ spectrum than on the PBH mass distribution, which is predominantly monochromatic. By observing the IGW spectral shape and the power law scaling in the UV frequency band one can infer the width and the amplitude of the scalar spectrum, the generator of the IGWs.

Consequently, we can say that the detection of the $\Omega_{\text{IGW}}(f)$ spectrum is a portal to the primordial power spectrum of curvature perturbations, $\mathcal{P}_{\mathcal{R}}(k)$. It can be used to discriminate inflationary models, and our analysis aimed at contributing to this direction.

ACKNOWLEDGMENTS

We would like to thank A. Kehagias, C. Kouvaris and A. Riotto for discussions. The work of I.D. is supported by IKY Scholarship, cofinanced by Greece and the European Union (European Social Fund), through the Operational Program "Human Resources Development, Education and Lifelong Learning" in the context of the project

⁸ Note that our ϵ is $\sqrt{2}\Delta$ in [52].

“Reinforcement of Postdoctoral Researchers - 2nd Cycle” (MIS-5033021), implemented by the State Scholarships Foundation.

Appendix A: GWs during kination era and constraints on the $\mathcal{P}_{\mathcal{R}}(k)$ and the reheating temperature.

The gravitational wave energy density gets enhanced during the kination regime [109–112]. The energy density of the GWs does not alter BBN predictions if

$$I \equiv h^2 \int_{k_{\text{BBN}}}^{k_{\text{max}}} \Omega_{\text{GW}}(k, \eta_0) d \ln k \leq 2 \times 10^{-6}. \quad (\text{A1})$$

Equivalently, the above constraint can be written in terms of the $\Omega_{\text{GW}}(k, \eta_c)$. The duration of the kination era is constrained due to energy density of the runaway field φ and the GWs, see [113–115] for a recent discussion in this context. Here, we derive a bound on the duration of the kination era coming from the amplitude of the IGWs, thus the $\mathcal{P}_{\mathcal{R}}(k)$ at small scales, see also [42, 53]. Let us assume that the energy of GWs is stored mainly in a narrow wave band (k_1, k_2) with central wave number k_p that enters the horizon at η_{entry} . During kination regime the GW energy density parameter scales as $\Omega_{\text{GW}} \propto a^2$. At the time of reheating it is

$$\Omega_{\text{GW}}(\eta_{\text{rh}}) \simeq \frac{1}{2} \frac{\rho_{\text{GW}}(\eta_{\text{entry}})}{\rho_{\text{tot}}(\eta_{\text{entry}})} \left(\frac{a(\eta_{\text{rh}})}{a(\eta_{\text{entry}})} \right)^2$$

where we assumed equipartition of energy densities at T_{rh} ; in the case of sudden transition, the 1/2 factor should be dropped. Therefore, $\Omega_{\text{GW}}(\eta_c) \simeq \Omega_{\text{GW}}(\eta_{\text{rh}}) \simeq \frac{1}{2} \Omega_{\text{GW}}(\eta_{\text{entry}}) (k_p/k_{\text{rh}})$. Let us make the top-hat approximation for the GW spectrum, $\Omega_{\text{GW}} = A_{\text{GW}}$ in the interval (k_1, k_2) . Then, the integral (A1) can be estimated. Plugging in numbers we find approximately the constraint

$$\frac{k_p}{k_{\text{rh}}} A_{\text{GW}} \ln \left(\frac{k_2}{k_1} \right) \lesssim 0.4. \quad (\text{A2})$$

For a ballpark analytic estimation, let us assume the GW spectrum width $k_2/k_1 = 10$ and consider the scaling $\Omega_{\text{GW}}(\eta_c) \sim A_{\mathcal{R}}^2$ during radiation domination era.

From the relation $k_{\text{rh}} = 2 \times 10^7 (T_{\text{rh}}/\text{GeV}) \text{Mpc}^{-1}$ and the kination era relation $k_p = 5.4 \times 10^{28} g_*^{-1/6} (T_{\text{rh}}/\text{GeV})^{-1/3} (M/\text{g})^{-2/3} \gamma^{2/3} \text{Mpc}^{-1}$, see Eq. (28), a rough conservative lower bound on the reheating temperature for the kination regime is found,

$$T_{\text{rh}} \gtrsim 10^7 \text{GeV} A_{\mathcal{R}}^{3/2} \left(\frac{M_{\text{hor}}}{10^{20} \text{g}} \right)^{-1/2}, \quad (\text{A3})$$

where $A_{\mathcal{R}} \equiv \mathcal{P}_{\mathcal{R}}(k_p)$. If this bound is violated, the BBN predictions are endangered.

Appendix B: Explicit PBH generating inflation models

In inflationary cosmology the primordial perturbations are produced from quantum fluctuations with a vast range of wave lengths. Here, we briefly present two sort of inflationary models that generate an enhanced amplitude for the $\mathcal{P}_{\mathcal{R}}(k)$ at small scales: the α -attractors [48, 49] and the GNMDC inflation models [50, 116].

1. α -attractors inflation

In the α -attractors inflation scenario [44], the effective Lagrangian for the inflaton field φ turns out to be

$$\frac{\mathcal{L}}{\sqrt{-g}} = \frac{1}{2} R - \frac{1}{2} \left(\partial_\mu \varphi \right)^2 - f^2 \left(\tanh \frac{\varphi}{\sqrt{6\alpha}} \right), \quad (\text{B1})$$

where $\text{Re}\Phi = \sqrt{3} \tanh(\varphi/\sqrt{6\alpha})$ is a chiral superfield, and R is the Ricci scalar. We also took $M_{\text{Pl}} = 1$. The canonically normalized inflaton potential that determines the inflationary trajectory is $V(\varphi) = f^2 (\tanh \varphi/\sqrt{6\alpha})$. Polynomial, trigonometric and exponential forms for the function $f(\text{Re}\Phi)$ can feature an inflection point plateau sufficient to generate a significant dark matter abundance in accordance with the observational constraints [48]. In this work we presented tensor power spectra induced by scalar power spectra $\mathcal{P}_{\mathcal{R}}(k)$ predicted by the inflationary potentials

$$V(\varphi) = f_0^2 \left[\sum_{n=0}^3 c_n \left(\tanh(\varphi/\sqrt{6\alpha}) \right)^n \right]^2 \quad (\text{B2})$$

and

$$V(\varphi) = f_0^2 \left[c_0 + c_1 e^{\lambda_1 \tanh \varphi/\sqrt{6}} + c_2 e^{\lambda_2 (\tanh(\varphi/\sqrt{6}) - \tanh(\varphi_P/\sqrt{6}))} \right]^2. \quad (\text{B3})$$

The form of the potentials (B2) and (B3) is depicted in Fig. 7. The inflection point plateau is the field region where the curvature perturbations get enhanced. The potential (B2) implements an RD cosmological postinflationary phase with high reheating temperature together with large amplitudes for $\mathcal{P}_{\mathcal{R}}(k)$ that induce GWs. The potential (B3) implements an inflationary phase followed by a kination phase. The kination phase can end gradually, as in the original proposal [49], or via a sudden transition due to e.g. an extra field direction toward a global minimum. The power spectra generated are depicted in Fig. 4. Details about the range of the parameter values for the inflationary models (B2) and (B3) as well details about the reheating temperature and the $\mathcal{P}_{\mathcal{R}}(k)$ amplitude and the PBH abundances can be found in the works [48] and [49].

PBH Mass	$\mathcal{P}_{\mathcal{R}}(k)$ type	$A_{\mathcal{R}}$	$\Omega_{\text{PBH}}/\Omega_{\text{DM}}$	$h^2 \Omega_{\text{IGW}}$	$f_{\text{p,IGW}}$	Experiment
10^{18} g	Gaussian 0.1	1.3×10^{-1}	$\mathcal{O}(1)$	9.3×10^{-10}	1.4×10^{-1} Hz	DECIGO + WD/Lensing
	Gaussian 1	4.1×10^{-2}		3.3×10^{-9}	1.4×10^{-1} Hz	
	α -attractors #1	2.1×10^{-2}		1.1×10^{-9}	9.1×10^{-2} Hz	
	Galileon	2.5×10^{-2}		1.1×10^{-9}	1.4×10^{-1} Hz	
10^{22} g	Gaussian 0.1	1.5×10^{-1}	$\mathcal{O}(1)$	1.4×10^{-9}	1.2×10^{-3} Hz	LISA + Lensing
	Gaussian 1	4.8×10^{-2}		4.4×10^{-9}	1.5×10^{-3} Hz	
10^{35} g	Gaussian 0.1	2.2×10^{-1}	$\mathcal{O}(10^{-5})$	8.9×10^{-9}	4.0×10^{-10} Hz	PTA + Lensing, X-rays
	Gaussian 1	6.2×10^{-2}		2.6×10^{-8}	4.1×10^{-10} Hz	

TABLE II. The values for the PBHs and the associated IGWs produced during *radiation* domination are listed. The types of $\mathcal{P}_{\mathcal{R}}(k)$ are listed together with the $A_{\mathcal{R}}$, the amplitude of the $\mathcal{P}_{\mathcal{R}}(k)$ peak, and an estimation of the produced PBH abundance. $h^2 \Omega_{\text{IGW}} = h^2 \int d \ln f \Omega_{\text{IGW}}(t_0, f)$ is the present total energy density value. The $f_{\text{p,IGW}}$ is the frequency that the IGW energy density peaks. In the last column we quote the experiments that probe each scenario.

PBH Mass	$\mathcal{P}_{\mathcal{R}}(k)$ type	A_0	$\Omega_{\text{PBH}}/\Omega_{\text{DM}}$	T_{rh}	$h^2 \Omega_{\text{IGW}}$	$f_{\text{p,IGW}}$	Experiment
10^{18} g	δ -distribution	1.6×10^{-2}	$\mathcal{O}(1)$	10^6 GeV	6.2×10^{-8}	1.1×10^{-1} Hz	DECIGO + WD/Lensing
		1.2×10^{-2}	$\mathcal{O}(10^{-5})$	5×10^4 GeV	1.3×10^{-6}	5.4×10^{-1} Hz	
10^{22} g		1.7×10^{-2}	$\mathcal{O}(10^{-1})$	10^4 GeV	1.1×10^{-6}	1.0×10^{-3} Hz	LISA + Lensing
		1.5×10^{-2}		5×10^2 GeV	2.2×10^{-6}	4.2×10^{-3} Hz	
10^{35} g			2.3×10^{-2}	$\mathcal{O}(10^{-5})$	0.01 GeV	3.1×10^{-8}	5.5×10^{-10} Hz

TABLE III. As in Table II, the values for the PBHs and the associated IGWs produced during *kination* domination are listed. The A_0 is the coefficient of the δ distribution and T_{rh} the reheating temperature for each scenario.

f_{hor}	$\mathcal{P}_{\mathcal{R}}(k)$ type	$A_{\mathcal{R}}$	M_{PBH}	β_{PBH}	$h^2 \Omega_{\text{IGW}}$	$f_{\text{p,IGW}}$	Experiment
10^2 Hz	Gaussian 0.1	7.8×10^{-2}	7×10^{12} g	$\mathcal{O}(10^{-24})$	3.4×10^{-10}	1.1×10^2 Hz	LIGO
	Gaussian 1	2.5×10^{-2}			1.2×10^{-9}	1.0×10^2 Hz	
	α -attractors #2	2.0×10^{-2}			1.9×10^{-10}	3.7×10^1 Hz	
10^{-1} Hz	Gaussian 0.1	9.0×10^{-2}	7×10^{18} g	$\mathcal{O}(10^{-22})$	4.5×10^{-10}	1.1×10^{-1} Hz	DECIGO
	Gaussian 1	2.7×10^{-2}			1.4×10^{-9}	1.0×10^{-1} Hz	
	α -attractors #2	1.4×10^{-2}			5.2×10^{-10}	3.4×10^{-2} Hz	
10^{-3} Hz	Gaussian 0.1	8.7×10^{-2}	7×10^{22} g	$\mathcal{O}(10^{-20})$	4.2×10^{-10}	1.1×10^{-3} Hz	LISA
	Gaussian 1	3.0×10^{-2}			1.7×10^{-9}	1.0×10^{-3} Hz	
10^{-9} Hz	Gaussian 0.1	1.2×10^{-1}	7×10^{34} g	$\mathcal{O}(10^{-16})$	1.7×10^{-9}	1.1×10^{-9} Hz	PTA
	Gaussian 1	3.8×10^{-2}			5.9×10^{-9}	1.0×10^{-9} Hz	

TABLE IV. The values for IGWs produced during *radiation* domination with zero or negligible PBH abundance, $\Omega_{\text{PBH}}/\Omega_{\text{DM}} \sim 10^{-10}$. The parameters are as in Table II. The $\beta(M)$ values are listed, Eq. (27), since PBHs with mass $M \lesssim 10^{15}$ g have already evaporated.

f_{hor}	$\mathcal{P}_{\mathcal{R}}(k)$ type	A_0	M_{PBH}	β_{PBH}	T_{rh}	$h^2 \Omega_{\text{IGW}}$	$f_{\text{p,IGW}}$	Experiment
10^2 Hz	δ -distribution	9×10^{-3}	10^{13} g	$\mathcal{O}(10^{-25})$	10^9 GeV	5.3×10^{-9}	$7.1 \times 10^1 \text{ Hz}$	LIGO
		4×10^{-4}	$5 \times 10^{14} \text{ g}$	$\mathcal{O}(10^{-550})$	10^6 GeV	1.7×10^{-8}	$6.2 \times 10^1 \text{ Hz}$	
10^{-1} Hz		8.8×10^{-3}	$5 \times 10^{20} \text{ g}$	$\mathcal{O}(10^{-26})$	10^3 GeV	2.3×10^{-6}	$3.1 \times 10^{-2} \text{ Hz}$	DECIGO
10^{-3} Hz		10^{-2}	$6 \times 10^{24} \text{ g}$	$\mathcal{O}(10^{-24})$	10 GeV	2.2×10^{-6}	$3.1 \times 10^{-4} \text{ Hz}$	LISA
10^{-9} Hz		1.5×10^{-2}	10^{35} g	$\mathcal{O}(10^{-16})$	0.02 GeV	7.7×10^{-9}	$1.6 \times 10^{-9} \text{ Hz}$	PTA

TABLE V. As in Table IV, the values for IGWs produced during *kination* domination for different reheating temperatures and with zero or negligible PBH abundance, $\Omega_{\text{PBH}}/\Omega_{\text{DM}} \sim 10^{-10}$, are listed.

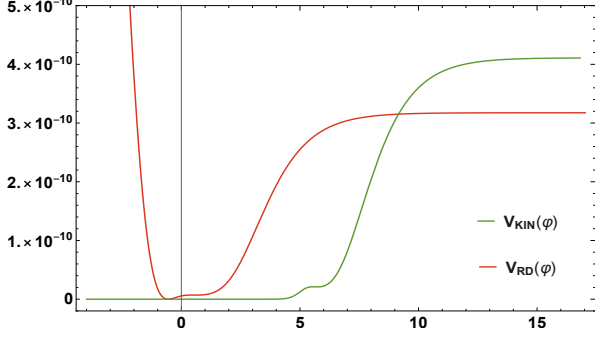


FIG. 7. The figure depicts the α -attractors inflationary potentials that generate CMB anisotropies, enhanced small-scale perturbations that trigger PBH formation, and induced GWs. A reheating phase follows inflation for the potential in red and a kination phase for the potential in green. The amplitude of the potential in green has been adjusted to fit in the same plot.

2. Horndeski GNMDC inflation

Horndeski theories are scalar-tensor theories of gravity [45, 46]. The Horndeski inflation model that we examine is the one with the nonminimal derivative coupling of the scalar field to the Einstein tensor, with a general φ -dependent form for the function $G_5(\varphi, X) = \hat{f}(\varphi)$ that is part of the generalized Galileon action [47]. This term was named general non-minimal derivative coupling (GNMDC) in [50]. The inflaton action is given by Eq. (18) and the potential that we use is

$$V(\varphi) = \frac{\lambda}{4} \varphi^4 \quad (\text{B4})$$

that can be identified with the Higgs [50]. The form of the GNMDC is

$$\hat{f}(\varphi) = \frac{\alpha \varphi^{\alpha-1}}{M^{\alpha+1}} (1 + f_{II}(\varphi)) , \quad (\text{B5})$$

with $f_{II} = d(((\varphi - \varphi_0)/s)^2 + 1)^{-1/2}$ that features a sharp peak at φ_0 [116]. The parameters s and d determine, respectively, the width and the amplitude of the f_{II} term.

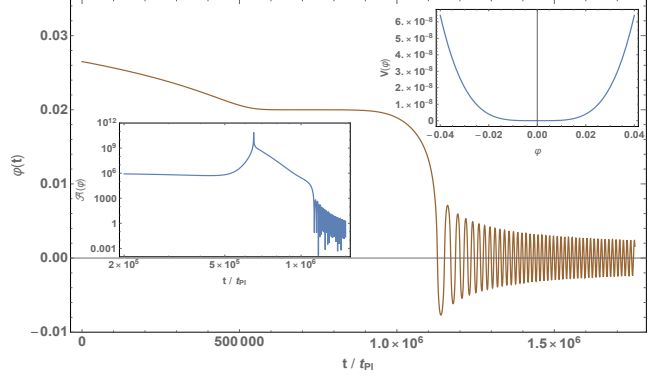


FIG. 8. The main plot depicts the evolution of the inflaton field with GNMDC. The inner plots depict a Higgs-like potential that together with the field-dependent GNMDC, $A(\varphi) = 1 + 3H^2 \hat{f}(\varphi)$ generates a peak in the $\mathcal{P}_{\mathcal{R}}(k)$, a PBH abundance, and induced GWs.

The GNMDC inflation features a noncanonical kinetic term that acts like friction, decelerating the inflaton field about the φ_0 value, while the field rolls down the $\lambda\varphi^4$ potential. The form of the GNMDC enhances significantly the $\mathcal{P}_{\mathcal{R}}(k)$ and triggers PBH formation [50]. The evolution of the inflaton scalar field with a Higgs-like potential is depicted in Fig. 8 when a field-dependent GNMDC, called $\mathcal{A}(\varphi)$, acts.

-
- [1] Sachiko Kuroyanagi, Takeshi Chiba, and Tomo Takahashi, “Probing the Universe through the Stochastic Gravitational Wave Background,” *JCAP* **11**, 038 (2018), arXiv:1807.00786 [astro-ph.CO].
- [2] Nelson Christensen, “Stochastic Gravitational Wave Backgrounds,” *Rept. Prog. Phys.* **82**, 016903 (2019), arXiv:1811.08797 [gr-qc].
- [3] Chiara Caprini and Daniel G. Figueroa, “Cosmological Backgrounds of Gravitational Waves,” *Class. Quant. Grav.* **35**, 163001 (2018), arXiv:1801.04268 [astro-ph.CO].
- [4] Sabino Matarrese, Ornella Pantano, and Diego Saez, “A General relativistic approach to the nonlinear evolution of collisionless matter,” *Phys. Rev. D* **47**, 1311–1323 (1993).
- [5] Sabino Matarrese, Silvia Mollerach, and Marco Bruni, “Second order perturbations of the Einstein-de Sitter universe,” *Phys. Rev. D* **58**, 043504 (1998), arXiv:astro-ph/9707278.
- [6] Hyerim Noh and Jai-chan Hwang, “Second-order perturbations of the Friedmann world model,” *Phys. Rev. D* **69**, 104011 (2004).
- [7] Carmelita Carbone and Sabino Matarrese, “A Unified treatment of cosmological perturbations from super-horizon to small scales,” *Phys. Rev. D* **71**, 043508 (2005), arXiv:astro-ph/0407611.
- [8] Kouji Nakamura, “Second-order gauge invariant cosmological perturbation theory: Einstein equations in terms of gauge invariant variables,” *Prog. Theor. Phys.* **117**, 17–74 (2007), arXiv:gr-qc/0605108.
- [9] Silvia Mollerach, Diego Harari, and Sabino Matarrese, “CMB polarization from secondary vector and tensor modes,” *Phys. Rev. D* **69**, 063002 (2004), arXiv:astro-ph/0310711.
- [10] Kishore N. Ananda, Chris Clarkson, and David Wands, “The Cosmological gravitational wave background from primordial density perturbations,” *Phys. Rev. D* **75**, 123518 (2007), arXiv:gr-qc/0612013.
- [11] Hooshyar Assadullahi and David Wands, “Gravitational waves from an early matter era,” *Phys. Rev. D* **79**, 083511 (2009), arXiv:0901.0989 [astro-ph.CO].
- [12] Daniel Baumann, Paul J. Steinhardt, Keitaro Takahashi, and Kiyotomo Ichiki, “Gravitational Wave Spectrum Induced by Primordial Scalar Perturbations,” *Phys. Rev. D* **76**, 084019 (2007), arXiv:hep-th/0703290.
- [13] Ryo Saito and Jun’ichi Yokoyama, “Gravitational wave background as a probe of the primordial black hole abundance,” *Phys. Rev. Lett.* **102**, 161101 (2009), [Erratum: *Phys. Rev. Lett.* **107**, 069901 (2011)], arXiv:0812.4339 [astro-ph].
- [14] Ioannis Dalianis, “Constraints on the curvature power spectrum from primordial black hole evaporation,” *JCAP* **08**, 032 (2019), arXiv:1812.09807 [astro-ph.CO].
- [15] Alba Kalaja, Nicola Bellomo, Nicola Bartolo, Daniele Bertacca, Sabino Matarrese, Ilia Musco, Alvise Raccanelli, and Licia Verde, “From Primordial Black Holes Abundance to Primordial Curvature Power Spectrum (and back),” *JCAP* **10**, 031 (2019), arXiv:1908.03596 [astro-ph.CO].
- [16] Bernard Carr, Kazunori Kohri, Yuuiti Sendouda, and Jun’ichi Yokoyama, “Constraints on Primordial Black Holes,” (2020), arXiv:2002.12778 [astro-ph.CO].
- [17] Misao Sasaki, Teruaki Suyama, Takahiro Tanaka, and Shuichiro Yokoyama, “Primordial black holes—perspectives in gravitational wave astronomy,” *Class. Quant. Grav.* **35**, 063001 (2018), arXiv:1801.05235 [astro-ph.CO].
- [18] E.V. Bugaev and P.A. Klimai, “Bound on induced gravitational wave background from primordial black holes,” *JETP Lett.* **91**, 1–5 (2010), arXiv:0911.0611 [astro-ph.CO].
- [19] R. Saito and J. Yokoyama, “Gravitational-wave constraints on the abundance of primordial black holes,” *Progress of Theoretical Physics* **123**, 867–886 (2010).
- [20] Edgar Bugaev and Peter Klimai, “Induced gravitational wave background and primordial black holes,” *Phys. Rev. D* **81**, 023517 (2010), arXiv:0908.0664 [astro-ph.CO].
- [21] Edgar Bugaev and Peter Klimai, “Constraints on the induced gravitational wave background from primordial black holes,” *Phys. Rev. D* **83**, 083521 (2011), arXiv:1012.4697 [astro-ph.CO].
- [22] Tomohiro Nakama, Joseph Silk, and Marc Kamionkowski, “Stochastic gravitational waves associated with the formation of primordial black holes,” *Phys. Rev. D* **95**, 043511 (2017), arXiv:1612.06264 [astro-ph.CO].
- [23] Nicholas Orlofsky, Aaron Pierce, and James D. Wells, “Inflationary theory and pulsar timing investigations of primordial black holes and gravitational waves,” *Phys. Rev. D* **95**, 063518 (2017), arXiv:1612.05279 [astro-ph.CO].
- [24] Juan Garcia-Bellido, Marco Peloso, and Caner Unal, “Gravitational Wave signatures of inflationary models from Primordial Black Hole Dark Matter,” *JCAP* **09**, 013 (2017), arXiv:1707.02441 [astro-ph.CO].
- [25] Rong-gen Cai, Shi Pi, and Misao Sasaki, “Gravitational Waves Induced by non-Gaussian Scalar Perturbations,” *Phys. Rev. Lett.* **122**, 201101 (2019), arXiv:1810.11000 [astro-ph.CO].
- [26] Keisuke Inomata and Tomohiro Nakama, “Gravitational waves induced by scalar perturbations as probes of the small-scale primordial spectrum,” *Phys. Rev. D* **99**, 043511 (2019), arXiv:1812.00674 [astro-ph.CO].
- [27] José Ramón Espinosa, Davide Racco, and Antonio Riotto, “A Cosmological Signature of the SM Higgs Instability: Gravitational Waves,” *JCAP* **09**, 012 (2018), arXiv:1804.07732 [hep-ph].
- [28] N. Bartolo, V. De Luca, G. Franciolini, M. Peloso, D. Racco, and A. Riotto, “Testing primordial black holes as dark matter with LISA,” *Phys. Rev. D* **99**, 103521 (2019), arXiv:1810.12224 [astro-ph.CO].
- [29] Christian T. Byrnes, Philippa S. Cole, and Subodh P. Patil, “Steepest growth of the power spectrum and primordial black holes,” *JCAP* **06**, 028 (2019), arXiv:1811.11158 [astro-ph.CO].
- [30] Yi-Fu Cai, Chao Chen, Xi Tong, Dong-Gang Wang, and Sheng-Feng Yan, “When Primordial Black Holes from Sound Speed Resonance Meet a Stochastic Background of Gravitational Waves,” *Phys. Rev. D* **100**, 043518 (2019), arXiv:1902.08187 [astro-ph.CO].

- [31] Sai Wang, Takahiro Terada, and Kazunori Kohri, “Prospective constraints on the primordial black hole abundance from the stochastic gravitational-wave backgrounds produced by coalescing events and curvature perturbations,” *Phys. Rev. D* **99**, 103531 (2019), [Erratum: *Phys.Rev.D* 101, 069901 (2020)], arXiv:1903.05924 [astro-ph.CO].
- [32] Jinn-Ouk Gong, “Analytic integral solutions for induced gravitational waves,” (2019), arXiv:1909.12708 [gr-qc].
- [33] Rafid Mahbub, “Primordial black hole formation in inflationary α -attractor models,” *Phys. Rev. D* **101**, 023533 (2020), arXiv:1910.10602 [astro-ph.CO].
- [34] Ogan Özsoy and Gianmassimo Tasinato, “On the slope of curvature power spectrum in non-attractor inflation,” *JCAP* **04**, 048 (2020), arXiv:1912.01061 [astro-ph.CO].
- [35] N. Bartolo, D. Bertacca, V. De Luca, G. Franciolini, S. Matarrese, M. Peloso, A. Ricciardone, A. Riotto, and G. Tasinato, “Gravitational wave anisotropies from primordial black holes,” *JCAP* **02**, 028 (2020), arXiv:1909.12619 [astro-ph.CO].
- [36] Matteo Braglia, Dhiraj Kumar Hazra, Fabio Finelli, George F. Smoot, L. Sriramkumar, and Alexei A. Starobinsky, “Generating PBHs and small-scale GWs in two-field models of inflation,” (2020), arXiv:2005.02895 [astro-ph.CO].
- [37] Guillermo Ballesteros, Julián Rey, Marco Taoso, and Alfredo Urbano, “Primordial black holes as dark matter and gravitational waves from single-field polynomial inflation,” (2020), arXiv:2001.08220 [astro-ph.CO].
- [38] Atsuhisa Ota, “Induced superhorizon tensor perturbations from anisotropic non-Gaussianity,” *Phys. Rev. D* **101**, 103511 (2020), arXiv:2001.00409 [astro-ph.CO].
- [39] Rouzbeh Allahverdi *et al.*, “The First Three Seconds: a Review of Possible Expansion Histories of the Early Universe,” (2020), arXiv:2006.16182 [astro-ph.CO].
- [40] Keisuke Inomata, Kazunori Kohri, Tomohiro Nakama, and Takahiro Terada, “Enhancement of gravitational waves induced by scalar perturbations due to a sudden transition from an early matter era to the radiation era,” *Proceedings, 16th International Conference on Topics in Astroparticle and Underground Physics (TAUP 2019): Toyama, Japan*, *J. Phys. Conf. Ser.* **1468**, 012002 (2020).
- [41] Keisuke Inomata, Kazunori Kohri, Tomohiro Nakama, and Takahiro Terada, “Gravitational waves induced by scalar perturbations during a gradual transition from an early matter era to the radiation era,” *Proceedings, 16th International Conference on Topics in Astroparticle and Underground Physics (TAUP 2019): Toyama, Japan*, *J. Phys. Conf. Ser.* **1468**, 012001 (2020).
- [42] Guillem Domènech, “Induced gravitational waves in a general cosmological background,” (2019), 10.1142/S0218271820500285, arXiv:1912.05583 [gr-qc].
- [43] Guillem Domènech, Shi Pi, and Misao Sasaki, “Induced gravitational waves as a probe of thermal history of the universe,” (2020), arXiv:2005.12314 [gr-qc].
- [44] Renata Kallosh, Andrei Linde, and Diederik Roest, “Superconformal Inflationary α -Attractors,” *JHEP* **11**, 198 (2013), arXiv:1311.0472 [hep-th].
- [45] Gregory Walter Horndeski, “Second-order scalar-tensor field equations in a four-dimensional space,” *Int. J. Theor. Phys.* **10**, 363–384 (1974).
- [46] Tsutomu Kobayashi, “Horndeski theory and beyond: a review,” *Rept. Prog. Phys.* **82**, 086901 (2019), arXiv:1901.07183 [gr-qc].
- [47] C. Deffayet, Xian Gao, D.A. Steer, and G. Zahariade, “From k-essence to generalised Galileons,” *Phys. Rev. D* **84**, 064039 (2011), arXiv:1103.3260 [hep-th].
- [48] Ioannis Dalianis, Alex Kehagias, and George Tringas, “Primordial black holes from α -attractors,” *JCAP* **01**, 037 (2019), arXiv:1805.09483 [astro-ph.CO].
- [49] Ioannis Dalianis and George Tringas, “Primordial black hole remnants as dark matter produced in thermal, matter, and runaway-quintessence postinflationary scenarios,” *Phys. Rev. D* **100**, 083512 (2019), arXiv:1905.01741 [astro-ph.CO].
- [50] Ioannis Dalianis, Stelios Karydas, and Eleftherios Papantonopoulos, “Generalized Non-Minimal Derivative Coupling: Application to Inflation and Primordial Black Hole Production,” *JCAP* **06**, 040 (2020), arXiv:1910.00622 [astro-ph.CO].
- [51] Rong-Gen Cai, Shi Pi, and Misao Sasaki, “Universal infrared scaling of gravitational wave background spectra,” (2019), arXiv:1909.13728 [astro-ph.CO].
- [52] Shi Pi and Misao Sasaki, “Gravitational Waves Induced by Scalar Perturbations with a Lognormal Peak,” (2020), arXiv:2005.12306 [gr-qc].
- [53] Kazunori Kohri and Takahiro Terada, “Semianalytic calculation of gravitational wave spectrum nonlinearly induced from primordial curvature perturbations,” *Phys. Rev. D* **97**, 123532 (2018), arXiv:1804.08577 [gr-qc].
- [54] Keitaro Tomikawa and Tsutomu Kobayashi, “Gauge dependence of gravitational waves generated at second order from scalar perturbations,” *Phys. Rev. D* **101**, 083529 (2020), arXiv:1910.01880 [gr-qc].
- [55] Juan Garcia-Bellido and Ester Ruiz Morales, “Primordial black holes from single field models of inflation,” *Phys. Dark Univ.* **18**, 47–54 (2017), arXiv:1702.03901 [astro-ph.CO].
- [56] Cristiano Germani and Tomislav Prokopec, “On primordial black holes from an inflection point,” *Phys. Dark Univ.* **18**, 6–10 (2017), arXiv:1706.04226 [astro-ph.CO].
- [57] Hayato Motohashi and Wayne Hu, “Primordial Black Holes and Slow-Roll Violation,” *Phys. Rev. D* **96**, 063503 (2017), arXiv:1706.06784 [astro-ph.CO].
- [58] Guillermo Ballesteros and Marco Taoso, “Primordial black hole dark matter from single field inflation,” *Phys. Rev. D* **97**, 023501 (2018), arXiv:1709.05565 [hep-ph].
- [59] Cristiano Germani and Alex Kehagias, “New Model of Inflation with Non-minimal Derivative Coupling of Standard Model Higgs Boson to Gravity,” *Phys. Rev. Lett.* **105**, 011302 (2010), arXiv:1003.2635 [hep-ph].
- [60] Sachiko Kuroyanagi, Kazunori Nakayama, and Jun’ichi Yokoyama, “Prospects of determination of reheating temperature after inflation by DECIGO,” *PTEP* **2015**, 013E02 (2015), arXiv:1410.6618 [astro-ph.CO].
- [61] Nicolás Bernal and Fazlollah Hajkarim, “Primordial Gravitational Waves in Nonstandard Cosmologies,” *Phys. Rev. D* **100**, 063502 (2019), arXiv:1905.10410 [astro-ph.CO].
- [62] Bernard J. Carr and S.W. Hawking, “Black holes in the early Universe,” *Mon. Not. Roy. Astron. Soc.* **168**, 399–415 (1974).
- [63] P. Meszaros, “The behaviour of point masses in an expanding cosmological substratum,” *Astron. Astrophys.* **37**, 225–228 (1974).

- [64] Bernard J. Carr, “The Primordial black hole mass spectrum,” *Astrophys. J.* **201**, 1–19 (1975).
- [65] D. Lindley, “A COLD BIG BANG WITH SMALL BLACK HOLES,” in *International School of Nuclear Physics: Nuclear Astrophysics* (1980) pp. 279–283.
- [66] Don N. Page and S.W. Hawking, “Gamma rays from primordial black holes,” *Astrophys. J.* **206**, 1–7 (1976).
- [67] Jane H. MacGibbon and Bernard J. Carr, “Cosmic rays from primordial black holes,” *Astrophys. J.* **371**, 447–469 (1991).
- [68] Bernard J. Carr and J.H. MacGibbon, “Cosmic rays from primordial black holes and constraints on the early universe,” *Phys. Rept.* **307**, 141–154 (1998).
- [69] A. Barrau, G. Boudoul, and L. Derome, “An improved gamma-ray limit on the density of pbhs,” in *28th International Cosmic Ray Conference* (2003) pp. 1697–1699, arXiv:astro-ph/0304528.
- [70] B.J. Carr, Kazunori Kohri, Yuuiti Sendouda, and Jun’ichi Yokoyama, “Constraints on primordial black holes from the Galactic gamma-ray background,” *Phys. Rev. D* **94**, 044029 (2016), arXiv:1604.05349 [astro-ph.CO].
- [71] Basudeb Dasgupta, Ranjan Laha, and Anupam Ray, “Neutrino and positron constraints on spinning primordial black hole dark matter,” (2019), arXiv:1912.01014 [hep-ph].
- [72] A. Barnacka, J.F. Glicenstein, and R. Moderski, “New constraints on primordial black holes abundance from femtolensing of gamma-ray bursts,” *Phys. Rev. D* **86**, 043001 (2012), arXiv:1204.2056 [astro-ph.CO].
- [73] P. Tisserand *et al.* (EROS-2), “Limits on the Macho Content of the Galactic Halo from the EROS-2 Survey of the Magellanic Clouds,” *Astron. Astrophys.* **469**, 387–404 (2007), arXiv:astro-ph/0607207.
- [74] Hiroko Niikura *et al.*, “Microlensing constraints on primordial black holes with Subaru/HSC Andromeda observations,” *Nature Astron.* **3**, 524–534 (2019), arXiv:1701.02151 [astro-ph.CO].
- [75] Massimo Ricotti, Jeremiah P. Ostriker, and Katherine J. Mack, “Effect of Primordial Black Holes on the Cosmic Microwave Background and Cosmological Parameter Estimates,” *Astrophys. J.* **680**, 829 (2008), arXiv:0709.0524 [astro-ph].
- [76] Bernard Carr, Florian Kuhnel, and Marit Sandstad, “Primordial Black Holes as Dark Matter,” *Phys. Rev. D* **94**, 083504 (2016), arXiv:1607.06077 [astro-ph.CO].
- [77] Sebastien Clesse and Juan García-Bellido, “The clustering of massive Primordial Black Holes as Dark Matter: measuring their mass distribution with Advanced LIGO,” *Phys. Dark Univ.* **15**, 142–147 (2017), arXiv:1603.05234 [astro-ph.CO].
- [78] Simeon Bird, Ilias Cholis, Julian B. Muñoz, Yacine Ali-Haïmoud, Marc Kamionkowski, Ely D. Kovetz, Alvise Raccanelli, and Adam G. Riess, “Did LIGO detect dark matter?” *Phys. Rev. Lett.* **116**, 201301 (2016), arXiv:1603.00464 [astro-ph.CO].
- [79] Vivian Poulin, Pasquale D. Serpico, Francesca Calore, Sebastien Clesse, and Kazunori Kohri, “CMB bounds on disk-accreting massive primordial black holes,” *Phys. Rev. D* **96**, 083524 (2017), arXiv:1707.04206 [astro-ph.CO].
- [80] Pasquale D. Serpico, Vivian Poulin, Derek Inman, and Kazunori Kohri, “Cosmic microwave background bounds on primordial black holes including dark matter halo accretion,” *Phys. Rev. Res.* **2**, 023204 (2020), arXiv:2002.10771 [astro-ph.CO].
- [81] Daniele Gaggero, Gianfranco Bertone, Francesca Calore, Riley M. T. Connors, Mark Lovell, Sera Markoff, and Emma Storm, “Searching for Primordial Black Holes in the radio and X-ray sky,” *Phys. Rev. Lett.* **118**, 241101 (2017), arXiv:1612.00457 [astro-ph.HE].
- [82] Misao Sasaki, Teruaki Suyama, Takahiro Tanaka, and Shuichiro Yokoyama, “Primordial Black Hole Scenario for the Gravitational-Wave Event GW150914,” *Phys. Rev. Lett.* **117**, 061101 (2016), [Erratum: *Phys.Rev.Lett.* 121, 059901 (2018)], arXiv:1603.08338 [astro-ph.CO].
- [83] Yu N. Eroshenko, “Gravitational waves from primordial black holes collisions in binary systems,” *J. Phys. Conf. Ser.* **1051**, 012010 (2018), arXiv:1604.04932 [astro-ph.CO].
- [84] Martti Raidal, Ville Vaskonen, and Hardi Veermäe, “Gravitational Waves from Primordial Black Hole Mergers,” *JCAP* **09**, 037 (2017), arXiv:1707.01480 [astro-ph.CO].
- [85] B.P. Abbott *et al.* (LIGO Scientific, Virgo), “Search for Subsolar-Mass Ultracompact Binaries in Advanced LIGO’s First Observing Run,” *Phys. Rev. Lett.* **121**, 231103 (2018), arXiv:1808.04771 [astro-ph.CO].
- [86] Tomohiro Harada, Chul-Moon Yoo, and Kazunori Kohri, “Threshold of primordial black hole formation,” *Phys. Rev. D* **88**, 084051 (2013), [Erratum: *Phys.Rev.D* 89, 029903 (2014)], arXiv:1309.4201 [astro-ph.CO].
- [87] B.P. Abbott *et al.* (KAGRA, LIGO Scientific, VIRGO), “Prospects for Observing and Localizing Gravitational-Wave Transients with Advanced LIGO, Advanced Virgo and KAGRA,” *Living Rev. Rel.* **21**, 3 (2018), arXiv:1304.0670 [gr-qc].
- [88] B. Sathyaprakash *et al.*, “Scientific Objectives of Einstein Telescope,” *Class. Quant. Grav.* **29**, 124013 (2012), [Erratum: *Class.Quant.Grav.* 30, 079501 (2013)], arXiv:1206.0331 [gr-qc].
- [89] Naoki Seto, Seiji Kawamura, and Takashi Nakamura, “Possibility of direct measurement of the acceleration of the universe using 0.1-Hz band laser interferometer gravitational wave antenna in space,” *Phys. Rev. Lett.* **87**, 221103 (2001), arXiv:astro-ph/0108011.
- [90] Shuichi Sato *et al.*, “The status of DECIGO,” *J. Phys. Conf. Ser.* **840**, 012010 (2017).
- [91] Jeff Crowder and Neil J. Cornish, “Beyond LISA: Exploring future gravitational wave missions,” *Phys. Rev. D* **72**, 083005 (2005), arXiv:gr-qc/0506015.
- [92] Pau Amaro-Seoane *et al.* (LISA), “Laser Interferometer Space Antenna,” (2017), arXiv:1702.00786 [astro-ph.IM].
- [93] Jun Luo *et al.* (TianQin), “TianQin: a space-borne gravitational wave detector,” *Class. Quant. Grav.* **33**, 035010 (2016), arXiv:1512.02076 [astro-ph.IM].
- [94] G. Hobbs *et al.*, “The international pulsar timing array project: using pulsars as a gravitational wave detector,” *Class. Quant. Grav.* **27**, 084013 (2010), arXiv:0911.5206 [astro-ph.SR].
- [95] Gemma Janssen *et al.*, “Gravitational wave astronomy with the SKA,” *PoS AASKA14*, 037 (2015), arXiv:1501.00127 [astro-ph.IM].
- [96] B.S. Sathyaprakash and B.F. Schutz, “Physics, Astrophysics and Cosmology with Gravitational Waves,” *Living Rev. Rel.* **12**, 2 (2009), arXiv:0903.0338 [gr-qc].

- [97] Kent Yagi and Naoki Seto, “Detector configuration of DECIGO/BBO and identification of cosmological neutron-star binaries,” *Phys. Rev. D* **83**, 044011 (2011), [Erratum: *Phys.Rev.D* 95, 109901 (2017)], arXiv:1101.3940 [astro-ph.CO].
- [98] Shun-Jia Huang, Yi-Ming Hu, Valeriya Korol, Peng-Cheng Li, Zheng-Cheng Liang, Yang Lu, Hai-Tian Wang, Shenghua Yu, and Jianwei Mei, “Science with the TianQin Observatory: Preliminary Results on Galactic Double White Dwarf Binaries,” (2020), arXiv:2005.07889 [astro-ph.HE].
- [99] Zu-Cheng Chen, Chen Yuan, and Qing-Guo Huang, “Pulsar Timing Array Constraints on Primordial Black Holes with NANOGrav 11-Year Data Set,” *Phys. Rev. Lett.* **124**, 251101 (2020), arXiv:1910.12239 [astro-ph.CO].
- [100] Rong-Gen Cai, Shi Pi, Shao-Jiang Wang, and Xing-Yu Yang, “Pulsar Timing Array Constraints on the Induced Gravitational Waves,” *JCAP* **10**, 059 (2019), arXiv:1907.06372 [astro-ph.CO].
- [101] Fabio Capela, Maxim Pshirkov, and Peter Tinyakov, “Constraints on Primordial Black Holes as Dark Matter Candidates from Star Formation,” *Phys. Rev. D* **87**, 023507 (2013), arXiv:1209.6021 [astro-ph.CO].
- [102] Fabio Capela, Maxim Pshirkov, and Peter Tinyakov, “Constraints on primordial black holes as dark matter candidates from capture by neutron stars,” *Phys. Rev. D* **87**, 123524 (2013), arXiv:1301.4984 [astro-ph.CO].
- [103] Peter W. Graham, Surjeet Rajendran, and Jaime Varela, “Dark Matter Triggers of Supernovae,” *Phys. Rev. D* **92**, 063007 (2015), arXiv:1505.04444 [hep-ph].
- [104] Timothy D. Brandt, “Constraints on MACHO Dark Matter from Compact Stellar Systems in Ultra-Faint Dwarf Galaxies,” *Astrophys. J. Lett.* **824**, L31 (2016), arXiv:1605.03665 [astro-ph.GA].
- [105] Andrey Katz, Joachim Kopp, Sergey Sibiryakov, and Wei Xue, “Femtolensing by Dark Matter Revisited,” *JCAP* **12**, 005 (2018), arXiv:1807.11495 [astro-ph.CO].
- [106] Paulo Montero-Camacho, Xiao Fang, Gabriel Vasquez, Makana Silva, and Christopher M. Hirata, “Revisiting constraints on asteroid-mass primordial black holes as dark matter candidates,” *JCAP* **08**, 031 (2019), arXiv:1906.05950 [astro-ph.CO].
- [107] R. Abbott *et al.* (LIGO Scientific, Virgo), “GW190814: Gravitational Waves from the Coalescence of a 23 Solar Mass Black Hole with a 2.6 Solar Mass Compact Object,” *Astrophys. J.* **896**, L44 (2020), arXiv:2006.12611 [astro-ph.HE].
- [108] Valerie Domcke, Ryusuke Jinno, and Henrique Rubira, “Deformation of the gravitational wave spectrum by density perturbations,” (2020), arXiv:2002.11083 [astro-ph.CO].
- [109] Massimo Giovannini, “Production and detection of relic gravitons in quintessential inflationary models,” *Phys. Rev. D* **60**, 123511 (1999), arXiv:astro-ph/9903004.
- [110] Alain Riazuelo and Jean-Philippe Uzan, “Quintessence and gravitational waves,” *Phys. Rev. D* **62**, 083506 (2000), arXiv:astro-ph/0004156.
- [111] M. Yahiro, G.J. Mathews, K. Ichiki, T. Kajino, and M. Orito, “Constraints on cosmic quintessence and quintessential inflation,” *Phys. Rev. D* **65**, 063502 (2002), arXiv:astro-ph/0106349.
- [112] Latham A. Boyle and Alessandra Buonanno, “Relating gravitational wave constraints from primordial nucleosynthesis, pulsar timing, laser interferometers, and the CMB: Implications for the early Universe,” *Phys. Rev. D* **78**, 043531 (2008), arXiv:0708.2279 [astro-ph].
- [113] Konstantinos Dimopoulos and Charlotte Owen, “Quintessential Inflation with α -attractors,” *JCAP* **06**, 027 (2017), arXiv:1703.00305 [gr-qc].
- [114] Yashar Akrami, Renata Kallosh, Andrei Linde, and Valeri Vardanyan, “Dark energy, α -attractors, and large-scale structure surveys,” *JCAP* **06**, 041 (2018), arXiv:1712.09693 [hep-th].
- [115] Michal Artymowski, Olga Czerwinska, Zygmunt Lalak, and Marek Lewicki, “Gravitational wave signals and cosmological consequences of gravitational reheating,” *JCAP* **04**, 046 (2018), arXiv:1711.08473 [astro-ph.CO].
- [116] Chengjie Fu, Puxun Wu, and Hongwei Yu, “Primordial Black Holes from Inflation with Nonminimal Derivative Coupling,” *Phys. Rev. D* **100**, 063532 (2019), arXiv:1907.05042 [astro-ph.CO].